Tectonics®

RESEARCH ARTICLE
10.1029/2022TC007261

Key Points:

- Three end-member deformation modes for Tibetan lithosphere are produced by varying the width, thickness and strength of the Qaidam crust
- Strong crust-mantle coupling of the Qaidam Basin prevents southward lithospheric subduction of the Eastern Kunlun-Qaidam-Qilian terrane
- Our simulations provide a plausible explanation for the two phases of Cenozoic crustal deformation in northeastern Tibet

Supporting Information:

Supporting Information may be found in the online version of this article.

Correspondence to:

R. Xie,
xierx@sustech.edu.cn

Citation:

Xie, R., Chen, L., Yin, A., Xiong, X., Chen, Y. J., Guo, Z., & Wang, K. (2023). Two phases of crustal shortening in northeastern Tibet as a result of a stronger Qaidam lithosphere during the Cenozoic India–Asia collision. *Tectonics*, *42*, e2022TC007261. https://doi.org/10.1029/2022TC007261

Received 8 FEB 2022
Accepted 4 JAN 2023

Two Phases of Crustal Shortening in Northeastern Tibet as a Result of a Stronger Qaidam Lithosphere During the Cenozoic India–Asia Collision

Renxian Xie[1,2], Lin Chen[3], An Yin[4], Xiong Xiong[5], Yongshun John Chen[1,2], Zhen Guo[1], and Kai Wang[6]

[1]Department of Ocean Science and Engineering, Southern University of Science and Technology, Shenzhen, China, [2]Southern Marine Science and Engineering Guangdong Laboratory (Guangzhou), Shenzhen, China, [3]State Key Laboratory of Lithospheric Evolution, Institute of Geology and Geophysics, Chinese Academy of Sciences, Beijing, China, [4]Department of Earth, Planetary and Space Sciences, University of California, Los Angeles, Los Angeles, CA, USA, [5]School of Geophysics and Geomatics, China University of Geosciences, Wuhan, China, [6]State Key Laboratory of Geodesy and Earth's Dynamics, Innovation Academy for Precision Measurement Science and Technology, Chinese Academy of Sciences, Wuhan, China

Abstract Although two phases of Cenozoic crustal deformation in the Qilian Shan thrust belt of northeastern Tibet has been documented, their dynamic causes remain unclear. To address this issue, we investigate whether the mechanical strength of the Qaidam Basin, which is located between the Eastern Kunlun Range and the Qilian Shan, was a controlling factor for the observed deformation history by performing 2-D thermal–mechanical simulations. Our models consider the division of the Tibetan terranes (i.e., Qilian arc, Kunlun-Qaidam, Songpan-Ganzi, Qiangtang, and Lhasa, from north to south) bounded by suture zones. Simulation results show that weak suture zones in central Tibet can lead to peeling off and sinking of the mantle lithosphere beneath the Qiangtang and Songpan–Ganzi terranes. After lithospheric delamination, varying north-south width, thickness and strength of the Qaidam crust creates three end-member model results: (a) the mantle lithosphere of the Lhasa terrane delaminates while the mantle lithosphere beneath Eastern Kunlun-Qaidam terrane and the Qilian Shan thrust belt (KQQ) remains undeformed, (b) the Lhasa mantle lithosphere moves northward while the KQQ mantle lithosphere subducts southward, and (c) the Lhasa mantle lithosphere moves northward while lithospheric thickening occurs north of the Qaidam Basin. Our simulations show that pre-existing weaknesses in northeastern Tibet can be activated and deformed shortly after the onset of collision, and a second wave of deformation sweeps across northeastern Tibet after lithospheric delamination in northern Tibet.

1. Introduction

How the Tibetan Plateau has been constructed is central to understanding continent-continent collisional processes on Earth (Royden et al., 2008; Tapponnier et al., 2001; Yin, 2010; Yin & Harrison, 2000). Based on the observed two phases of post-collisional crustal deformation in northeastern Tibet (Figure 1), two end-member models have been proposed: (a) plateau has been developed progressively northward and reached northeastern Tibet at 20–15 Ma (e.g., England & Houseman, 1986; Meyer et al., 1998; Tapponnier et al., 2001), and (b) plateau formation occurred nearly synchronously across the northern and southern margins of Tibet since the onset of the India–Asia collision (Dupont–Nivet et al., 2004; Yin et al., 2002). The northward-plateau-growth model requires the Tibetan lithosphere to have a homogeneous mechanical property (e.g., England & Houseman, 1986) or a sequential reaction of pre-existing suture zones between pre-Cenozoic Tibetan terranes (Meyer et al., 1998; Tapponnier et al., 2001). In contrast, the early deformation hypothesis of northern Tibet requires a medium-strength Tibetan lithosphere (Huangfu et al., 2022). Therefore, although the formation of the Tibetan Plateau involved two phases of crustal deformation in northeastern Tibet, the mechanisms of deformation remain unclear.

It has long been known that the lithosphere of the Tibetan Plateau was deformed pervasively in the Cenozoic (Yin & Harrison, 2000). However, the presence of only thin-skinned thrust systems across the Qaidam Basin (Yin et al., 2008) implies that the basement of the basin has escaped Cenozoic deformation, and crustal structures and mechanical properties gleaned from geophysical data support this view (Figure 1; e.g., Karplus et al., 2011; Yang et al., 2012; Chen et al., 2015; Deng & Tesauro, 2016; Xiao et al., 2016). The observations note above raise the

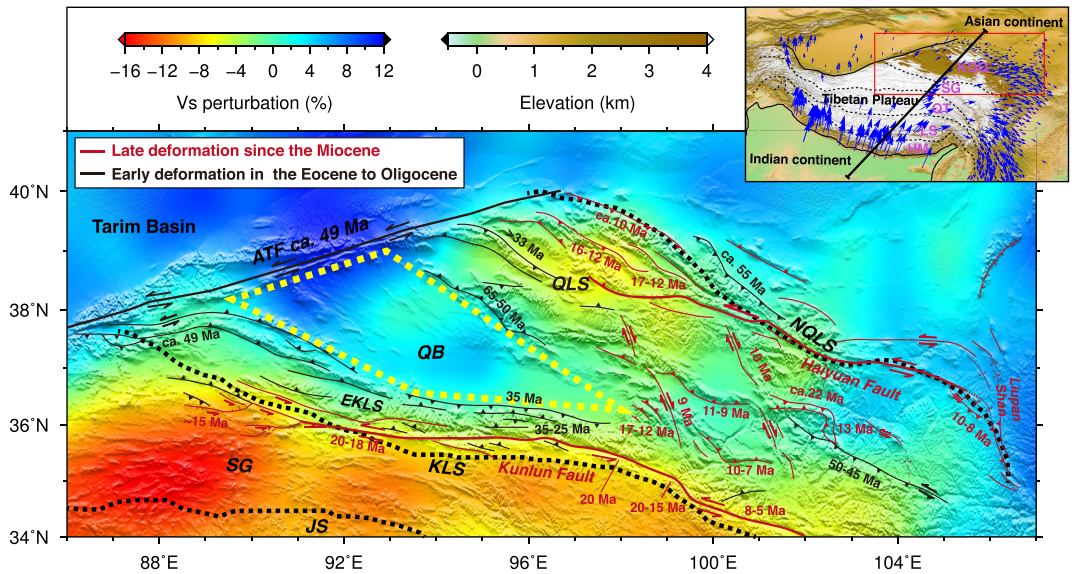

Figure 1. Two phases of tectonic deformation and deep crustal structure in northeastern Tibet. Structures in black are results of early phase deformation during the Eocene–Oligocene, and in red are results of late phase deformation initiated since the Miocene (e.g., Duvall et al., 2013). Background color indicates shear wave velocity structure at 30 km depth (Yang et al., 2012). The high-velocity Qaidam crust implies that it is stronger than the crust of the Songpan–Ganzi and the Qilian Shan terranes. The inset shows the multi-terrane Tibetan Plateau and the current crustal movement relative to the stable Eurasian continent (Zhang et al., 2004). The black thin dashed lines represent sutures, and the black thick line indicates roughly the cross section of our models, the observed topography, and lithosphere profile shown in Figures 11 and 12. In our numerical models, the whole Qaidam crust is represented by plagioclase, nevertheless, the upper and lower crust in other regions is represented by wet quartz and plagioclase, respectively. Weak sutures are represented by weakened wet quartz in the crustal part and wet olivine in the mantle-lithosphere part. All mantle lithospheres are represented by dry olivine, and a dense mantle lithosphere is adopted in the Tibetan Plateau. Abbreviations: ATF: Altyn Tagh fault; HM: Himalaya terrane; LS: Lhasa terrane; QT: Qiangtang terrane; SG: Songpan–Ganzi terrane; KQQ: Eastern Kunlun–Qaidam terrane and Qilian Shan thrust belt; EKLS: Eastern Kunlun Shan; QB: Qaidam basin; QLS: Qilian Shan; JS: Jinsha Suture; KLS: Kunlun Suture; NQLS: Northern Qilian Suture.

question of how a strong block within the Tibetan Plateau could assist stress transfer and the concentration of thick-skinned basement-involved deformation along its margins.

There are great uncertainties about the India–Asia collision, including its start time, the amount of Indian continental convergence, how these materials were absorbed, and the precursor phase of Neotethyan subduction (van Hinsbergen et al., 2012; Hu et al., 2016 and references therein). The Continental Greater India or Greater India Basin was thought to exit between the Indian continent and southern Asian margin and be completely subducted below the Himalaya terrane (van Hinsbergen et al., 2012; Hu et al., 2016; Ingalls et al., 2016). Whether large-scale Indian subduction has an impact on the far-end lithospheric deformation of the Tibetan Plateau also remains unclear.

Expanding on early work on the role of heterogeneous lithospheric rheology in controlling Tibetan deformation (Chen et al., 2017, 2020; Huangfu et al., 2018; Kelly et al., 2020; Kong et al., 1997), we present here a 2-D thermal–mechanical model that addresses specifically the role of the mechanical properties of the Qaidam crust in controlling the Cenozoic deformation history of northeastern Tibet. We performed two groups of models, one without subduction of the Continental Greater India, and the other with subduction of the Continental Greater India.

2. Geological Setting

The Qaidam Basin is bounded to the north by the Cenozoic Qilian–Nan Shan thrust belt that was reactivated along the early Paleozoic Qilian Orogen (e.g., Zuza et al., 2018 and references therein). The basin is bounded to the south by the Cenozoic Eastern Kunlun Shan transpressional fault system (Tapponnier et al., 2001; Yin et al., 2008; Figure 1). The Moho deepens southward from ~50 km beneath the Qaidam Basin to ~70 km beneath

the Eastern Kunlun Shan and the Songpan-Ganzi terrane (Karplus et al., 2011; Yang et al., 2012). To the north, the Moho depth increases to ~60 km in the Qilian Shan (Yang et al., 2012). Several mechanisms have been proposed for the Cenozoic tectonic development of the northeastern Tibetan Plateau, including lower-crustal channel flow and lower crustal injection (Clark & Royden, 2000; Karplus et al., 2011), southward subduction of the Qilian Shan mantle lithosphere (Meyer et al., 1998; Tapponnier et al., 2001), pure-shear lithospheric thickening (Zhang et al., 2020), and southward underthrusting of the North China mantle lithosphere (Ye et al., 2015; Zuza et al., 2019). Thermochronological studies have revealed multiple Cenozoic cooling phases in the Paleocene–Eocene, Eocene–Oligocene and middle–late Miocene (Duvall et al., 2013; Yuan et al., 2013). The segment of the Altyn Tagh fault bounding the northwestern margin of the Qaidam Basin and the thrust belts along the northeastern and southern margins of the basin were initiated at 60–50 Ma during or shortly after the initial India–Asia collision (Figure 1; Yin et al., 2008). However, an intense phase of deformation at 20–10 Ma may have prevailed across the Qilian Shan-Nan Shan thrust belt (Meyer et al., 1998; Tapponnier et al., 2001), which was marked by the initiation of several strike-slip faults in the region (Figure 1; e.g., Duvall et al., 2013; Yuan et al., 2013).

Cenozoic sediments in the Qaidam Basin are thickest in the west (>15 km) (Cheng et al., 2021; Yin et al., 2008), and the basin basement consisting of Proterozoic gneisses and early Paleozoic ultrahigh-pressure metamorphic rocks is exposed at the eastern end of the basin (Song et al., 2005; Yang et al., 2001). The lithologies of the basin basement are consistent with the felsic to intermediate crustal composition inferred from seismic studies (e.g., Xu et al., 2013; Zhao et al., 2013). The estimated ~70 km effective elastic thickness of the Qaidam Basin is 10–30 km thicker than the rest of the Tibetan Plateau (Chen et al., 2015). Magnetotelluric data have revealed a high-resistivity lower crust beneath the Eastern Kunlun Shan and southern Qaidam Basin, which may be indicative of a drier and stronger lower crust (Xiao et al., 2016).

3. Numerical Methods and Model Setup

We conducted numerical modeling using the thermal-mechanical code I2VIS (Gerya & Yuen, 2003a). This code adopts a finite-difference method with a full-staggered grid and marker-in-cell technique to solve the mass, momentum, and energy conservation equations while taking into account ductile–plastic rheology, partial melting of rock, and surface processes (also see Xie et al., 2021). Introductions about the governing equations, the partial melting of rock and surface processes are provided in Supporting Information S1. The lithospheric strength of the Qaidam Basin is a key test parameter in this study, and we discuss it more fully below.

3.1. Rheology of the Lithosphere

The lithosphere exhibits ductile and plastic behavior on geological time scales. Ductile deformation may be accommodated by dislocation and diffusion creep mechanisms. Viscosities for plastic power law dislocation creep and Newtonian diffusion creep are expressed as follows (Gerya, 2011):

$$\eta_{\mathrm{disl}} = \frac{1}{2}\frac{1}{(A_D)^{-1/n}(\dot{\varepsilon}_{II})^{(n-1)/n}}\exp\left(\frac{E_a + V_a P}{n\mathrm{RT}}\right) \times S, \tag{1}$$

$$\eta_{\mathrm{diff}} = \frac{1}{2}\frac{A_D}{\sigma_{cr}^{(n-1)}}\exp\left(\frac{E_a + V_a P}{\mathrm{RT}}\right) \times S, \tag{2}$$

where η_{disl} and η_{diff} are viscosities for dislocation and diffusion creep, respectively; $\dot{\varepsilon}_{\mathrm{II}} = (0.5\dot{\varepsilon}_{ij}\dot{\varepsilon}_{ij})^{1/2}$ is the second invariant of the strain rate tensor, and σ_{cr} is the critical stress for the dislocation to diffusion stress transition. The parameters A_D, E_a, V_a, and n are the material constant, activation energy, activation volume, and stress exponent, respectively. R is the universal gas constant. Finally, the strength factor, S, is introduced to vary the lithospheric viscosity of the Qaidam Basin (Beaumont et al., 2009).

For mineral aggregates, both dislocation and diffusion creep may occur simultaneously and the combined effective viscosity can be expressed as:

$$\frac{1}{\eta_{\mathrm{ductile}}} = \frac{1}{\eta_{\mathrm{disl}}} + \frac{1}{\eta_{\mathrm{diff}}}, \tag{3}$$

where η_{ductile} is the effective ductile viscosity.

Plastic rheology follows the Drucker-Prager yield criterion defined by

$$\begin{aligned} \eta_{\text{plastic}} &= \frac{\sigma_{\text{yield}}}{2\dot{\varepsilon}_{\text{II}}}, \\ \sigma_{\text{yield}} &= C_0 + P\sin(\varphi_{\text{eff}}), \\ \sin(\varphi_{\text{eff}}) &= \sin(\varphi)(1-\lambda), \end{aligned} \tag{4}$$

where σ_{yield}, C_0, φ, and λ are yield stress, cohesion, internal friction angle, and pore-fluid pressure ratio, respectively.

The lithospheric effective viscosity is taken from the minimum of the ductile versus plastic viscosities (Ranalli, 1995):

$$\eta_{\text{eff}} = \min\left(\eta_{\text{ductile}}, \eta_{\text{plastic}}\right). \tag{5}$$

Finally, the effective viscosity relates the deviatoric stress σ' to strain rate $\dot{\varepsilon}$ via the constitutive relationship of:

$$\sigma' = 2\eta_{\text{eff}}\dot{\varepsilon}. \tag{6}$$

3.2. Model Setup

Our 2-D numerical models were computed in a domain (Figure 2a) that is 4,000 km × 1,000 km and divided into 381 × 2,048 nodes in a cross-section view. Along the horizontal axis, stable nodes are spaced at 5 km in the marginal region and 1 km in the central region. In the vertical direction, the grid spacing for the upper 200 km is 1 km; it increases from 1 to 5 km for the depth range 200–300 km, and is 5 km for the depth below 300 km. Over 70 million Lagrangian markers were distributed randomly in the computational domain to trace the deformation.

Our models consider three tectonic units, that is, the Indian continent, the Tibetan Plateau and the Asian continent. We set five weak zones to represent the Indus–Yarlung Tsangpo Suture (IYS), the Bangong–Nujiang Suture (BNS), Jinsha Sture (JS), the Kunlun Suture (KLS), and North Qilian Suture (NQLS; Figure 2b). These suture zones with weak rheology are remnants of ancient subduction zones, and they play an important role in later lithospheric deformation (Heron et al., 2016; Xie et al., 2021). The geometric properties of the suture zones are inferred roughly from the main geological events, and the observational constraints and evidence are given in Text S2 in Supporting Information S1. These sutures bound the Lhasa, Qiangtang, Songpan–Ganzi, and Eastern Kunlun–Qaidam terrane and Qilian Shan thrust belt (KQQ) (Yin & Harrison, 2000). A strong crustal block as thick as the Tibetan crust is placed in the south of the KQQ terrane to represent the whole Qaidam crust (Figures 2d and 2e). Moreover, we simply assumed a 130 km thick initial lithosphere for the three continental blocks with a 30 km upper crust and a 20 km lower crust in the Tibetan Plateau, which is 10 km thicker than the crust of the Indian and Asian continents. The pre-thickened crust in the Tibetan Plateau is supported by observations of crustal thickening prior to the India–Asia collision (Murphy et al., 1997). We used wet quartz, plagioclase, and dry olivine flow laws to represent upper crust, lower crust, and mantle respectively. Weakened wet quartz and wet olivine were used to represent crustal and lithospheric sutures, respectively. The rheological parameters used in the model calculations are listed in Table 1, and strength factor S is 1 for all terranes except the Qaidam crust whose strength factor S will be tested. Following the work of Zhang et al. (2014), Goussin et al. (2020), and Ma et al. (2021), we assumed a metasomatic mantle–lithosphere lid beneath Tibet created in the late Mesozoic prior to the India–Asia collision. Based on the geochemical and petrological arguments of O'Reilly and Griffin (2013) for a metasomatized mantle, we further assumed the density of this fertile mantle–lithosphere lid beneath Tibet to be 50 kg/m^3 denser than normal mantle lithosphere. The other parameters used in the model are listed in Table 2.

The side and upper boundaries are free-slip, whereas the bottom boundary condition is permeable and governed by $\partial v_x/\partial y = 0$ and $\partial v_y/\partial y = v_y/\Delta y_{\text{external}}$ with v_x and v_y as the horizontal and vertical velocity components, and $\Delta y_{\text{external}}$ as the distance between the model bottom and external boundary. The external boundary is a virtual boundary and is located at a depth of 1,000 km away from the model bottom where free-slip conditions are satisfied. The permeable boundary allows mantle to convect, which solves the problem of the boundary effect at the base of the model. The thermal boundary conditions are as follows: the upper-boundary temperature is fixed at

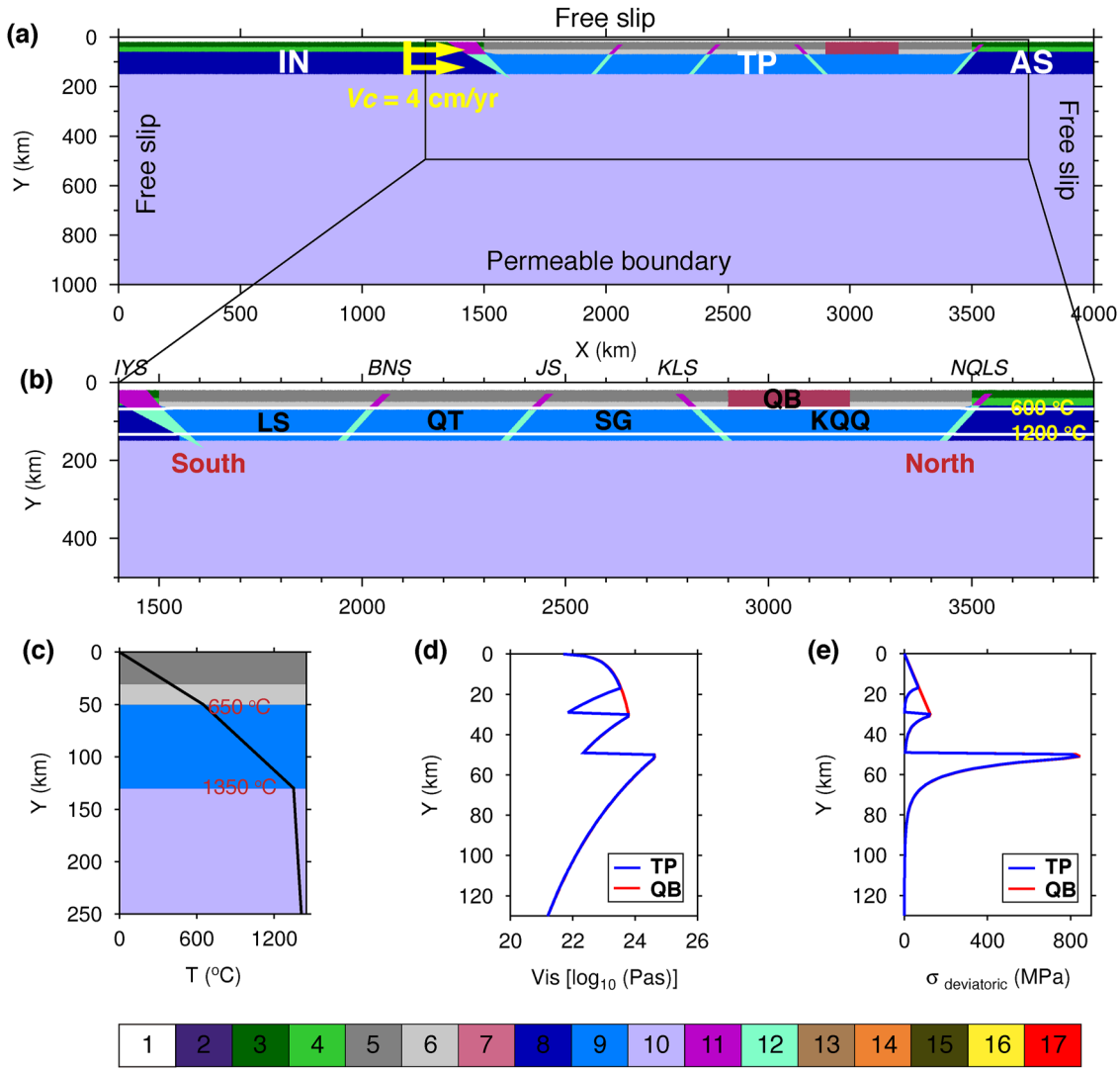

Figure 2. Model setup. (a) Global model and boundary conditions. Three tectonic units in the model are the Indian continent (IN), the Tibetan plateau (TP) and the Asian continent (AS). The yellow arrows indicate convergence rate of 4 cm/yr. (b) Enlarged study region. The two white lines are isotherms of 600 and 1200°C. (c) Initial geotherm of the Tibetan Plateau. (d). (e) Initial viscosities and corresponding deviatoric stress. The red and blue lines represent the initial strength of the Qaidam Basin and other regions in the Tibetan Plateau, respectively. When calculating the initial viscosity and converting it to deviatoric stress by constitutive relation, the strain rate is assumed to be 1×10^{-16} s^{-1}. Abbreviations: IYS: Indus–Yarlung Tsangpo suture; BNS: Bangong–Nujiang suture; other abbreviations refer to Figure 1. Colored grids for different rock types, with: 1–sticky air; 2–sediments; 3/4–upper/lower crust of the India and Asia; 5/6–upper/lower crust of the Tibetan plateau; 7–strong crustal block representing the Qaidam block; 8, 9–mantle lithosphere; 10–asthenosphere; 11/12–crustal/Lithospheric sutures; 13/14–partially molten upper/lower crust of the India and Asia; 15/16–partially molten upper/lower crust of the Tibetan plateau; 17–partially molten asthenosphere. The sediments and partially molten rocks are not shown in this figure, but will appear during the model evolution. Detailed properties of different rock types are shown in Tables 1 and 2.

0°C, the two sides of model have adiabatic boundaries with no horizontal heat flux across the vertical boundaries, and the bottom thermal boundary condition is defined by $\partial T/\partial y = (T_{\text{external}} - T)/\Delta y_{\text{external}}$, where T_{external} is a fixed temperature at 2280°C. As a permeable boundary, temperature and vertical heat fluxes can vary along the model bottom during model simulations. The crustal geothermal gradient is assumed to be 13°C/km, which requires the Moho temperature to be 650° and 520°C beneath the Tibetan Plateau and the two plateau-bounding blocks to the north and south, respectively (Figure 2c). We also set a temperature of 1350°C at the base of the Asian, Indian, and Tibetan lithospheres. An adiabatic thermal gradient of 0.5 °C/km is used for the asthenosphere. Furthermore, a 20 km thick "sticky air layer" is placed on the top of the model, which allows a realistic construction of topography during model simulations (Crameri et al., 2012; Schmeling et al., 2008). Finally, a constant 4 cm/yr convergence rate is applied to the Indian lithosphere in a profile with $X = 1{,}300$ km and $Y = 20$–140 km (Figure 2a). The assumed constant convergence rate is a simplification of the true convergence-rate history

Table 1
Rheological Parameters of Rocks Used in This Study

Rocks	Abbreviations	E_a (K J mol^{-1})	V_a (K J mol^{-1})	n	A_D (MPa^{-n} s^{-1})	η_0[a] (Pa^n s)	sin(φ_{eff})	C_0 (MPa)
Sticky air	SA	–	–	1	–	1.00×10^{18}	0	0
Wet quartzite	WQ	154	8	2.3	3.2×10^{-4}	1.97×10^{17}	0.15	1.0
Plagioclase	PL	238	12	3.2	3.2×10^{-4}	4.80×10^{22}	0.15	1.0
Diabase	DB	260	12	3.4	2.0×10^{-4}	1.26×10^{24}	0.15	1.0
Dry mafic granulite	DMG	238	12	4.2	3.3×10^{-4}	1.13×10^{21}	0.15	1.0
Dry olivine	DOL	532	12	3.5	2.5×10^{4}	3.98×10^{16}	0.6	1.0
Weakened Wet quartzite	WWQ	154	8	2.3	3.2×10^{-4}	1.97×10^{17}	0.05	0.1
Wet olivine	WOL	470	12	4.0	2.0×10^{3}	5.01×10^{20}	0.006	0.1
References	Karato et al. (1986); Wilks and Carter (1990); Ranalli (1995)							

[a]η_0 is the reference viscosity, which is calculated by $\eta_0 = (1/A_D) \times 10^{6n}$.

between India and Asia, which varies between 3 and 5 cm/yr (Cande et al., 2010; Meng et al., 2012; Molnar & Stock, 2009). However, we note that our assumed rate is similar to the average shortening rate of the Asian lithosphere at 3.4 cm/yr (Guillot et al., 2003).

4. Model Results

We performed a series of models to systematically assess the effect of width, thickness, and strength of the Qaidam crust on the deformation history of northeastern Tibet. All models show northward Indian-lithosphere underthrusting, lithospheric delamination and decompression melting beneath the northern plateau in the early stages of the model runs. In the later stages of the model runs, three lithospheric-deformation modes emerge

Table 2
Other Parameters Used in This Study[a]

Compositions	Rocks	ρ_0 (kgm^{-3})	K[b] (W/m/K)	T_s[c] (K)	T_l[d] (K)	H_L (KJ/kg)	H_r (uW/m^3)
Sticky air	–	1	–	–	–	–	0
Upper crust	WQ	2,700 (solid)	K1	TS1	TL1	300	1.5
		2,400 (molten)					
Lower crust	PL	2,800 (solid)	K2	TS2	TL2	380	0.25
		2,500 (molten)					
Mantle lithosphere	DOL	3,300 (solid)	K3	TS3	TL3	400	0.022
		3,350 (metasomatic)					
Asthenosphere	DOL	3,300 (solid)	K3	TS4	TL3	400	0.022
		2,900 (molten)					
Strong crustal block	PL	2,800	K2	TS2	TL2	380	0.25
Crustal suture	WWQ	2,700	K1	TS1	TL1	300	1.5
Lithospheric suture	WOL	3,300	K3	TS3	TL3	400	0.022
References[e]	1	2	3	4, 5	4	2, 6	2

[a]Other parameters: Heat capacity $Cp = 1000\,J\,kg^{-1}\,K^{-1}$, thermal expansion $\alpha = 3 \times 10^{-5}\,K^{-1}$, the compressibility $\beta = 1 \times 10^{-5}\,MPa^{-1}$; $\rho = \rho_0(1 - \alpha(T - T_0))(1 + \beta(P - P_0))$, where ρ_0 is initial density at standard conditions (T_0 = 20°C, P_0 = 10^5 MPa). [b]K1 = 0.64 + 807/(T + 77); $K2$ = 1.18 + 474/(T + 77); K3 = [0.73 + 1,293/(T + 77)] × (1 + 0.00004P). [c]TS1 = 889 + 17,900/(P + 54) + 20,200/(P + 54)^2, P < 1,200 MPa; or TS1 = 831 + 0.06P, P > 1,200 MPa. TS2 = 973 − 70400/(P+354)+77,800,000/(P+354)^2, P < 1,600 MPa; or TS2 = 935 + 0.0035P + 0.0000062P^2, P > 1,600 MPa. TS3 = 1,394 + 0.132899P − 0.000005104P^2, P < 10,000 MPa; or TS3 = 2,212 + 0.030819 × (P − 10000), P > 10,000 MPa. TS4 is the mantle solidus with 0.01% water content. TS4 = 689.32 + 221920P − 13.87 × 10^4P^2 + 3.3 × 10^8P^3, $P \leqq$ 14,870 MPa; TS4 = 2,199.24 − 35450P + 2.29 × 10^4P^2-3.8 × 10^7P^3, P > 15,170 MPa; TS4 = 457.74 + 105110P, 14,870 MPa < $P \leqq$ 15,170 MPa. [d]TL1 = 1,262 + 0.09P, TL2 = 1,423 + 0.105P, TL3 = 2,073 + 0.114P. [e]1 = Gerya (2011); 2 = Turcotte and Schubert (2014); 3 = Clauser and Huenges (1995); 4 = Schmidt and Poli (1998); 5 = Litasov et al. (2011); 6 = Bittner and Schmeling (1995).

Table 3
Tested Numerical Parameters and Model Results

Model name	Widths of QC (km)	Thicknesses of QC (km)	Strength factors of QC	Add a CGI?	Results (Figure)
Model 1	300	50	1	No	3 and 4
Models 2–4	50/400/700	50	1	No	5 and S2 in Supporting Information S1
Models 5–8	300	40/30/20/0	1	No	6 and S3 in Supporting Information S1
Models 9–11	300	50	0.1/0.5/10	No	7
Model 12	300	50	1	Yes	8
Model 13	300	50	10	Yes	13

Note. QC, Qaidam crust; CGI, the Continental Greater India.

while varying the width, thickness, and strength of the Qaidam crust: (a) the Lhasa lithosphere delaminates to the south and the KQQ lithosphere remains undeformed, (b) the Lhasa lithosphere continues to move northward and the KQQ lithosphere subducts southward, and (c) the Lhasa lithosphere continues to advance northward while the KQQ lithosphere region is thickened. Here we select 13 typical models (Models 1–11 without subduction of the Continental Greater India, Models 12 and 13 with subduction of the Continental Greater India) to display the simulation results in detail (Table 3).

4.1. Reference Model

In the reference model (Model 1), the Qaidam crust is assumed to be 300 km in the horizontal direction, and 50 km in the vertical direction, and to have a crustal strength factor of 1. The Qaidam crust is placed in the south of the KQQ terrane. The simulation results for this reference model show that during incipient collision, the Indian lithosphere underthrusts northward along the IYS, and that the Qiangtang and Songpan–Ganzi mantle lithosphere also underthrusts along the BNS, JS, and KLS, respectively (Figure 3a). Meanwhile, the deformation front propagates forward rapidly, generating high topography across the entire Tibetan Plateau. Lithospheric deformation is concentrated mainly to the south of the KQQ terrane owing to the resistance of the stronger Qaidam crust, and minor deformation occurs along the northern Qilian Shan margin (Figures 4a and 4b). Crustal thickening south of the modeled Qaidam crust leads to rapid uplift, and a basin is gradually developed above the basement (Figure 3b). The subducting lithosphere becomes denser relative to its surrounding mantle owing to its lower temperature (Figure 4c). As a result, the entire Qiangtang mantle lithosphere is peeled away from the crust, with this process being referred to as lithospheric delamination and being facilitated by partial melting in the mantle (Figure 3c). The Songpan–Ganzi mantle lithosphere is dragged into the deeper mantle by the delamination of the Qiangtang lithosphere. A lithospheric window is opened by delamination, resulting in asthenospheric upwelling and decompression melting. Upwelling of the hot asthenosphere heats the crust and causes partial melting of the upper crust (Figures 3c and 4d). Delamination of the mantle lithosphere in northern Tibet allows the Lhasa mantle lithosphere to be pushed northward more easily than before. Driven by the Indian continental subduction, lithospheric deformation in the Tibetan Plateau propagates northward, as expressed by crustal thickening in the northern KQQ terrane. The Qaidam crust is also pushed northward with little internal deformation. Meanwhile, the partially molten asthenosphere is pushed northward by the Lhasa mantle lithosphere. During this process, the partially molten asthenosphere gradually intrudes the basal section of the crust, which helps the crust decouple from the mantle lithosphere, and contributes to the southward subduction of the KQQ mantle lithosphere. When the crustal shortening in the Tibetan domain is as much as ~700 km, the Indian lithosphere becomes subducted northward beneath the BNS in the south, and the KQQ mantle lithosphere is bent downward like a subduction zone beneath the Qaidam region (Figure 3d).

4.2. Effect of the Qaidam Width

In this section, we test a series of models to assess the role of the north-south width of the Qaidam crust while holding other parameters constant. Figure 5 shows several snapshots of such models that display a similar evolutionary path to that of the reference model in the early stage of the model run. However, a remarkable difference in lithospheric deformation emerges in the later stages of model runs after the shared lithospheric delamination

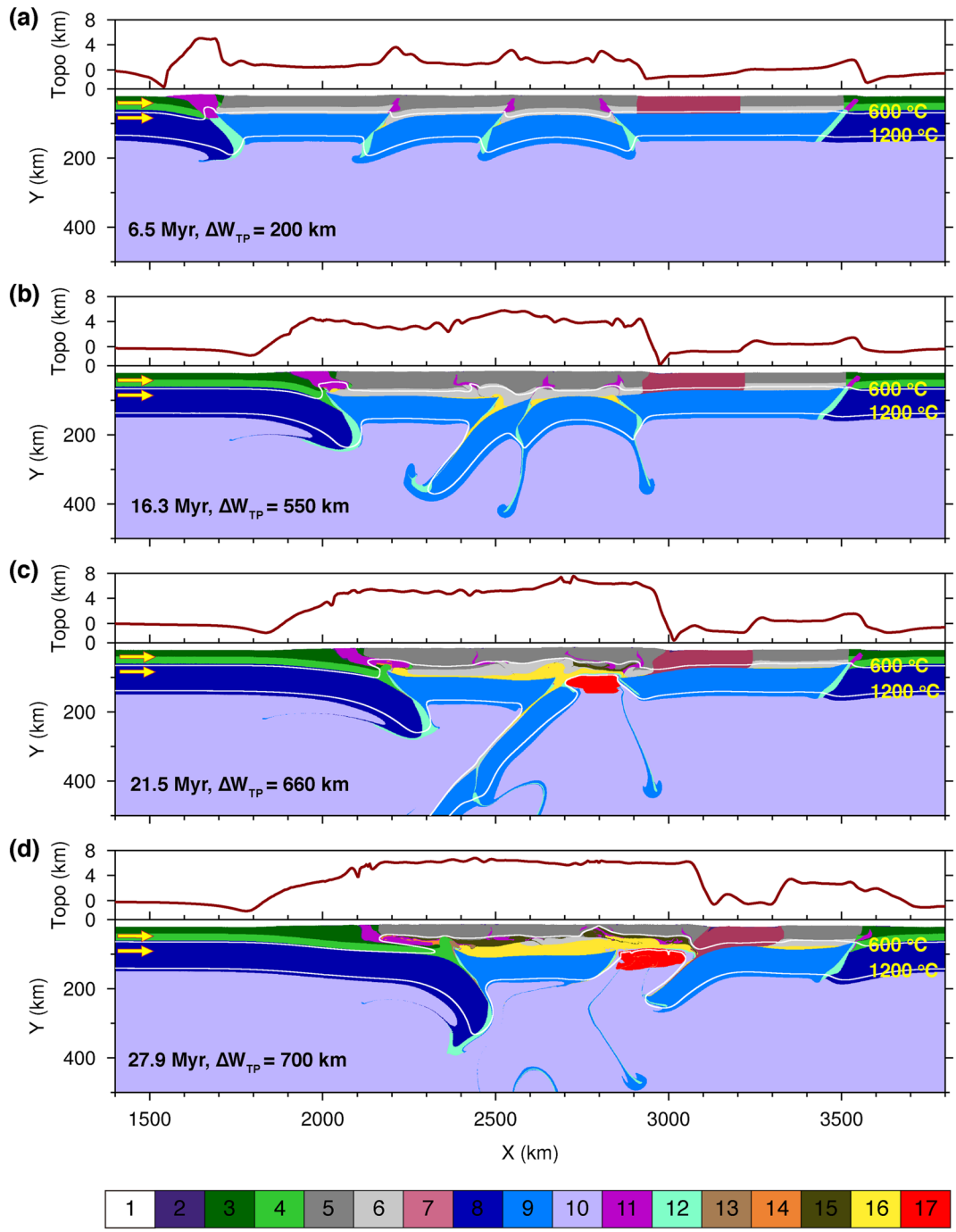

Figure 3. Simulation results of the reference model (Model 1). The Qaidam crust is assumed to be 300 km wide, and 50 km thick in the vertical direction, and to have a crustal strength factor of 1 in the reference model. (a–d) Topography and composition results at 6.5 Myr (ΔW_{TP} = 200 km), 16.3 Myr (ΔW_{TP} = 550 km), 21.5 Myr (ΔW_{TP} = 660 km), and 27.9 Myr (ΔW_{TP} = 700 km), respectively. ΔW_{TP} indicates the amount of crustal shortening to the north of the IYS. In each snapshot, the topography profile overlays on the composition field. Arrows indicate the moving direction of the Indian lithosphere, and the two white lines are isotherms of 600 and 1200°C.

event in the northern Tibetan Plateau. The Qaidam crust in Model 2 is 50 km wide, 1/14 the width of the KQQ region (Figure 5a). The narrow Qaidam crustal block cannot resist displacement, and it is pushed northward during lithospheric delamination below the Qiangtang and Songpan–Ganzi terranes. Meanwhile, the partially molten asthenosphere intrudes into the Lhasa crust, which facilitates the southward peeling of the Lhasa mantle

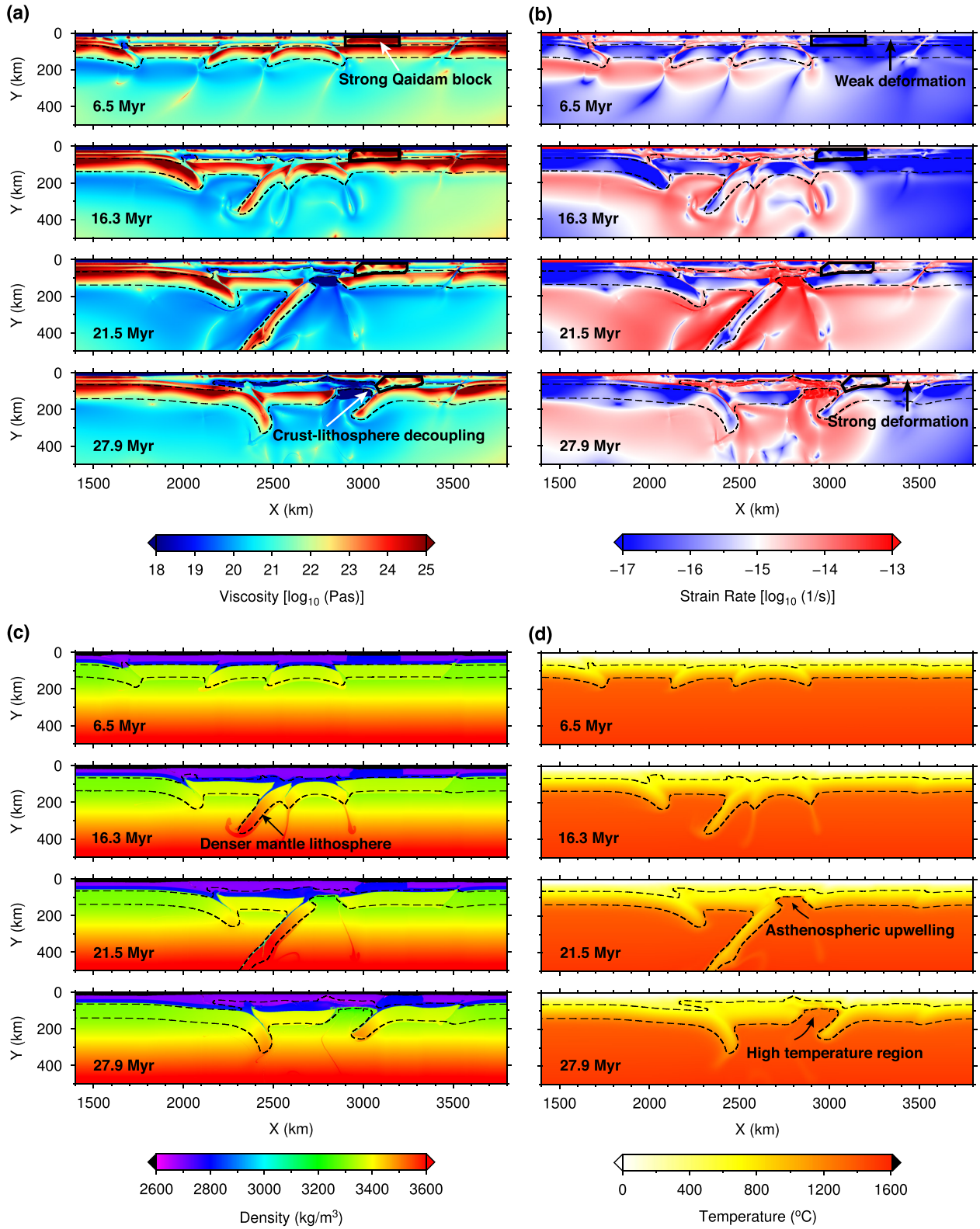

Figure 4. Viscosity, strain rate, density and temperature results of the reference model. (a) Viscosity field; (b) Strain rate field; (c) Density field and (d) Temperature field. The Qaidam crust is pointed out by the black polygon in (a and b). The two black lines are isotherms of 600° and 1200°C in each snapshot.

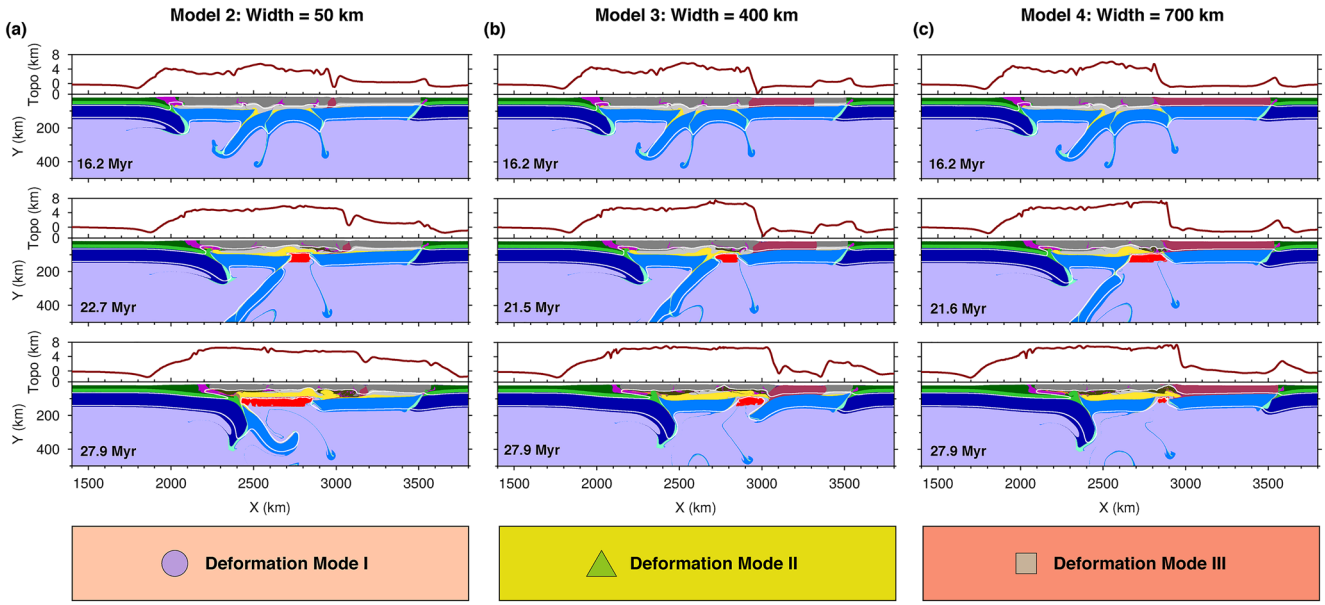

Figure 5. Simulation results of models with different Qaidam crustal widths. (a–c) Topography and composition results at different evolution time of Models 2–4. The Qaidam crust is 50 km, 400 and 700 km wide in Models 2–4, respectively. Three distinct lithospheric-deformation modes caused by Qaidam crust with different widths after lithospheric delamination. (a) The first mode (Deformation Mode I) is caused by a narrow Qaidam crust, and it is characterized by southward delamination of the LS mantle lithosphere and an undeformed KQQ mantle lithosphere. (b) The second mode (Deformation Mode II) is caused by a wide Qaidam crust, and it is characterized by northward-advancing LS mantle lithosphere and southward subduction of the KQQ mantle lithosphere. (c) The last mode (Deformation Mode III) is caused by an extremely wide Qaidam crust, and it is characterized by northward-advancing LS mantle lithosphere and undeformed KQQ mantle lithosphere.

lithosphere. Topography across the whole plateau is at a similar height, and a narrow and shallow basin is formed in the Qaidam region. The evolutionary path of Model 3 with a block 400 km width is similar to that of the reference model from the beginning to the end of the model runs (Figure 5b). Models with Qaidam crust widths of 150–650 km (2/14 to 13/14 the width of the KQQ terrane) also yield similar evolutionary paths to that of the reference model (Figure S2 in Supporting Information S1). We used Model 4 to represent a special case where the Qaidam crust is extremely wide (Figure 5c). In contrast, an extremely wide Qaidam crust results in little deformation across the Qaidam region, while the crust to the south is intensely shortened in association with high topography. The wide Qaidam crust also resists northward movement of the partially molten asthenospheric materials. Meanwhile, the window of mantle upwelling is closed by the progressive northward movement of the Lhasa mantle lithosphere. Model 4 shows that the system develops a lithospheric architecture expressed by northward subduction of the Indian lithosphere in the south, minor deformation of the KQQ lithosphere in the north, and a small window of mantle upwelling beneath the Songpan–Ganzi terrane.

4.3. Effect of the Qaidam Crustal Thickness

In this section, we describe a group of models to examine the effects of varying Qaidam crustal thickness. In the reference model, the thickness of the Qaidam crust is assumed to be 50 km, which is equal to the initial crustal thickness of the Tibetan Plateau. Here, we systematically decrease the Qaidam crustal thickness, while keeping all other parameters the same as those used in the reference model. Model 5 has a 40 km thick Qaidam crust, and its results are identical to the reference model (Figure 6a). Models 6, 7, and 8 involve a Qaidam crust that is 30, 20, and 0 km thick, respectively, and the results differ drastically from those of Models 1 and 5 but are similar to the results of Model 2 in that the Lhasa mantle lithosphere is delaminated southward after the delamination of the Qiangtang and Songpan–Ganzi mantle lithosphere (Figure 6b and Figure S3 in Supporting Information S1).

4.4. Effect of the Qaidam Crustal Strength

In this section, we run a couple of models to explore the effects of Qaidam crustal strength on lithospheric deformation. As shown in Equations 1–3, we used various strength factors S to scale the strength of the Qaidam crust in Models 9, 10, and 11 while keeping other parameters consistent with those in the reference model.

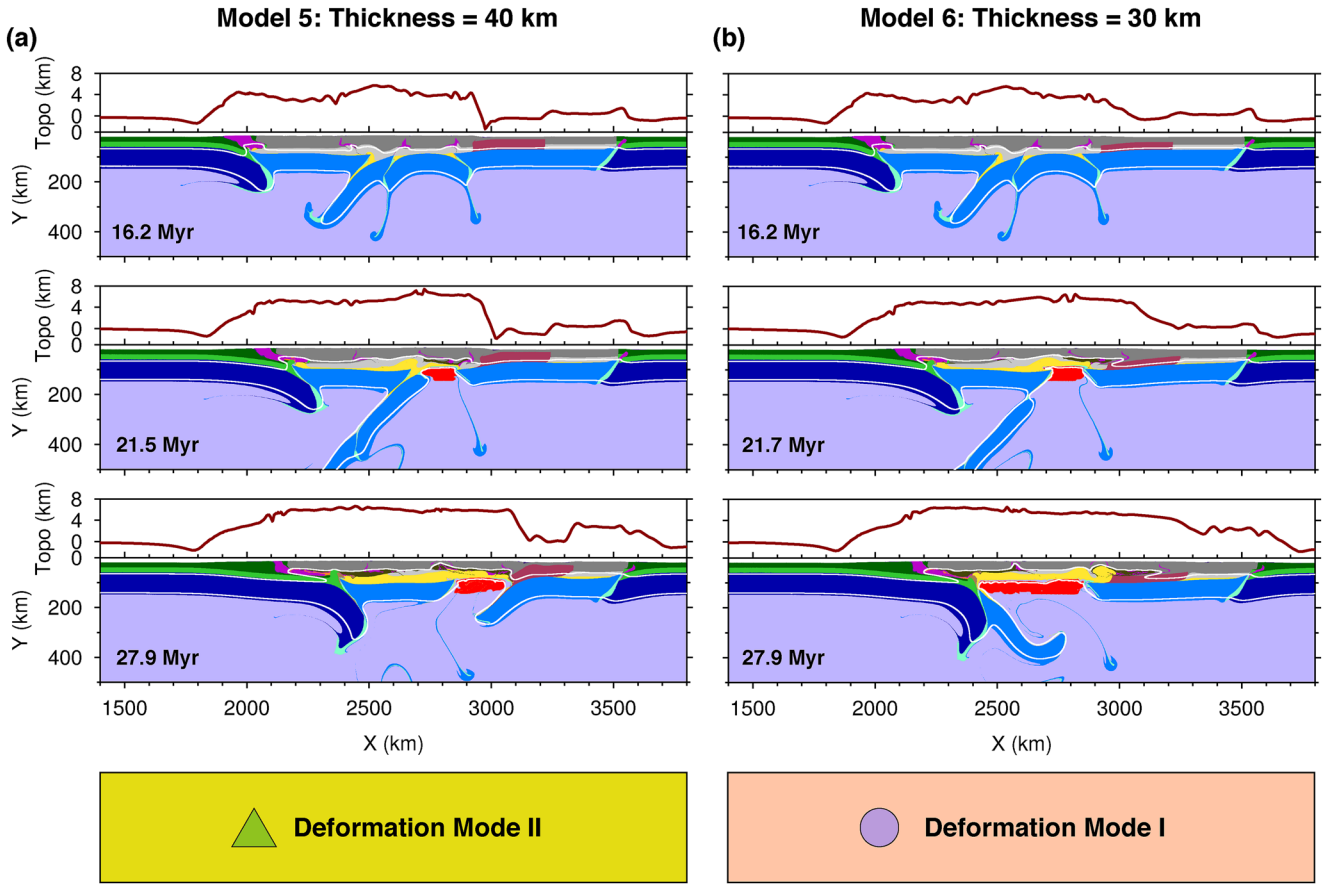

Figure 6. Simulation results of models with different Qaidam crustal thicknesses. (a–b) Topography and composition results at different evolution times of Model 5, 6. The Qaidam crustal thickness is 40 and 30 km in Models 5 and 6, respectively. Simulation results show two lithospheric deformation modes similar to Mode II (Model 5) and Mode I (Model 6).

Figure 7 shows the simulation results. Strength factor *S* plays a role in ductile rheology, therefore, and changing its value would mainly affect lower crustal strength where deformation is dominated by ductile rheology. Compared with the reference model, the initial lower crustal strength is reduced by an order of magnitude using a strength factor of 0.1 in Model 9. The simulation results show that a strong upper crust and the mantle lithosphere are decoupled by weak lower crust, expressed by the former moving faster than the latter. The results of Model 9 are similar to those in Models 2 and 6 (Figure 7a). The strength factor is 0.5 in Model 10, resulting in the lower crust having half the strength than it had in the reference model. Model 10 gives similar results to those of Model 1, 3, and 5 (Figure 7b). The strength factor in Model 11 is 10, and the crust is dominated by brittle strength, with the initial viscosity in the lowermost 10 km layer of crust one order of magnitude larger than that of the reference model. The strong crust and mantle lithosphere of the Qaidam crust are always strongly coupled, thus they behave as a rigid block that prevents the crustal deformation from propagating northward. The strengthened Qaidam crust plays a role that is similar to that of an extremely wide Qaidam crust. Hence, the evolution shown in Model 11 is analogous to that of Model 4 (Figure 7c). However, in the late stages of evolution in Model 11, the mantle lithosphere the north of the KQQ terrane is thickened after lithospheric delamination beneath the Qiangtang and Songpan-Ganzi terranes, which is more significant if there are more weak zones in this region (Figure S4a in Supporting Information S1). After systematically testing of the strength factors, three lithospheric-deformation modes can be distinguished, which are similar to those caused by varying width of the Qaidam crust.

4.5. Effect of the Subduction-Consumed Continental Greater India

In Models 1–11, the India–Asia collision begins immediately after model initiation. In Model 12, we add an 1,100 km terrane with a thin crust of 15 km and mantle lithosphere of 90 km to represent the Continental Greater

10.1029/2022TC007261

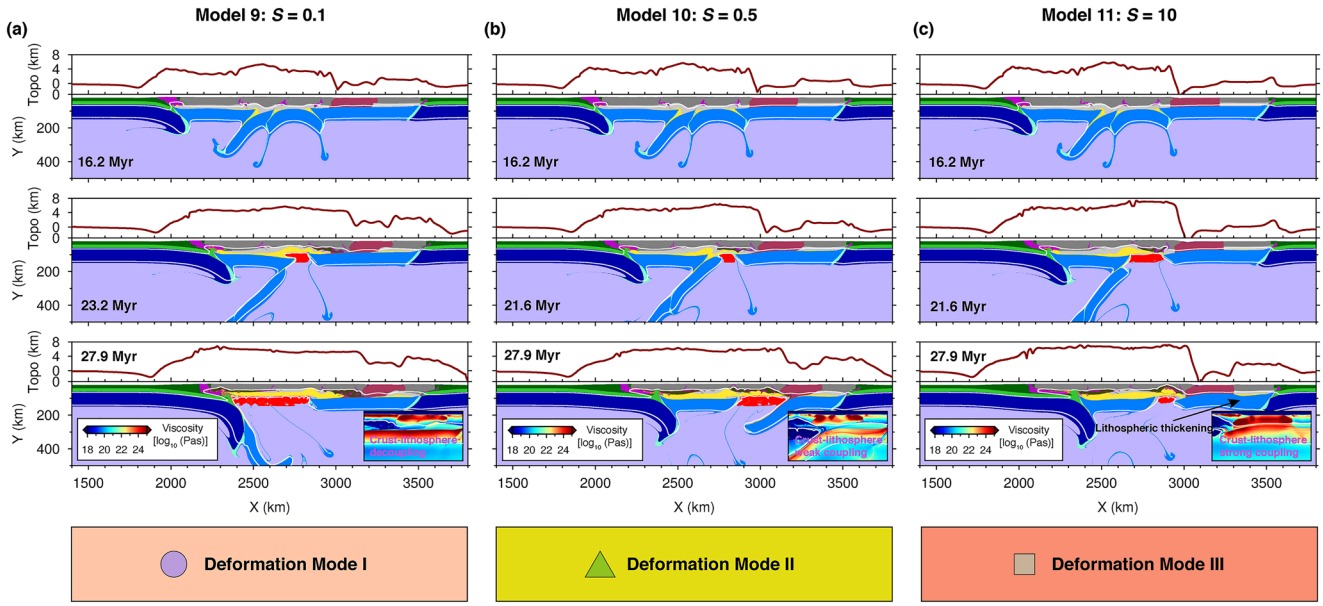

Figure 7. Simulation results of models with different Qaidam crustal strengths. (a–c) Topography and composition results at different evolution times of Models 9–11. The insets are viscosity results at 27.9 Myr in the Qaidam region. The crustal strength factor is 0.1, 0.5 and 10 in Models 9–11, respectively. Similar three lithospheric-deformation modes are caused by a weakened, normal and strengthened Qaidam crust, respectively. But in Model 11, the mantle lithosphere is thickened to the north of the Qaidam region, which is slightly different from Figure 5c.

India. To facilitate the subduction of the Continental Greater India, the density of the Continental Greater India mantle lithosphere is 50 kg/m^3 denser than that of the Indian mantle lithosphere. Other Parameters are same to the Indian continent. As shown in Figure 8, in the early stage of model evolution, the Continental Greater India lithosphere subducts deeply to the mantle and breaks off at 28.3 Myr. During this phase, crustal shortening in the Tibetan Plateau is about 173 km, and topography uplifts to ∼1.3 km in the whole Tibetan Plateau except the Qaidam region where an intermountain basin gradually forms. After subduction of the Continental Greater India, the Indian lithosphere indents the Tibetan lithosphere, subsequent model results are similar to the reference model, but with less shortening in the Tibetan lithosphere when model terminates at 52.1 Myr.

5. Discussion

5.1. Three Lithospheric Deformation Modes

In all of our models, mantle lithosphere of the Qiangtang terrane is first to underthrust and delaminate in the early stage, which is similar to the evolution described by Kelly et al. (2020). However, in contrast to their results, our models predict three distinct deformation modes after lithospheric delamination in northern Tibet as a result of changing the crustal properties of the Qaidam Basin (Figure 9a).

The first deformation mode (Deformation Mode I) features southward delamination of the Lhasa mantle lithosphere and a relatively undeformed KQQ mantle lithosphere. If the Qaidam crust is narrow (width ratio <1/7), or weak (crustal strength factor <0.2), or thin (strong crustal thickness <30 km), it has no capacity to resist deformation. In this situation, the Qaidam crust is prone to being pushed northward relative to the underlying mantle lithosphere which remains in place in the early evolution of the model (e.g., Model 9 in Figure 9b-I). As a result, the relative horizontal displacement between them gradually increases, which implies crust–mantle lithosphere decoupling in the Qaidam region (e.g., Model 9 in Figures 9b-II). Crustal deformation and strain partitioning in the Qaidam region delay lithospheric delamination below the Songpan–Ganzi terranes. Slow sinking of the Songpan–Ganzi mantle lithosphere helps the partially molten asthenosphere intrude the lower crust of the Lhasa terrane, triggering southward delamination of the Lhasa mantle lithosphere (Figures 5a, 6b, and 7a). The second deformation mode (Deformation Mode II) features northward-advanced Lhasa mantle lithosphere and flexing of the mantle lithosphere beneath the Qaidam region. If the Qaidam crust is wide, or if the crustal strength factor reaches 1.0, the Qaidam crust and the mantle lithosphere are slightly coupled (e.g.,

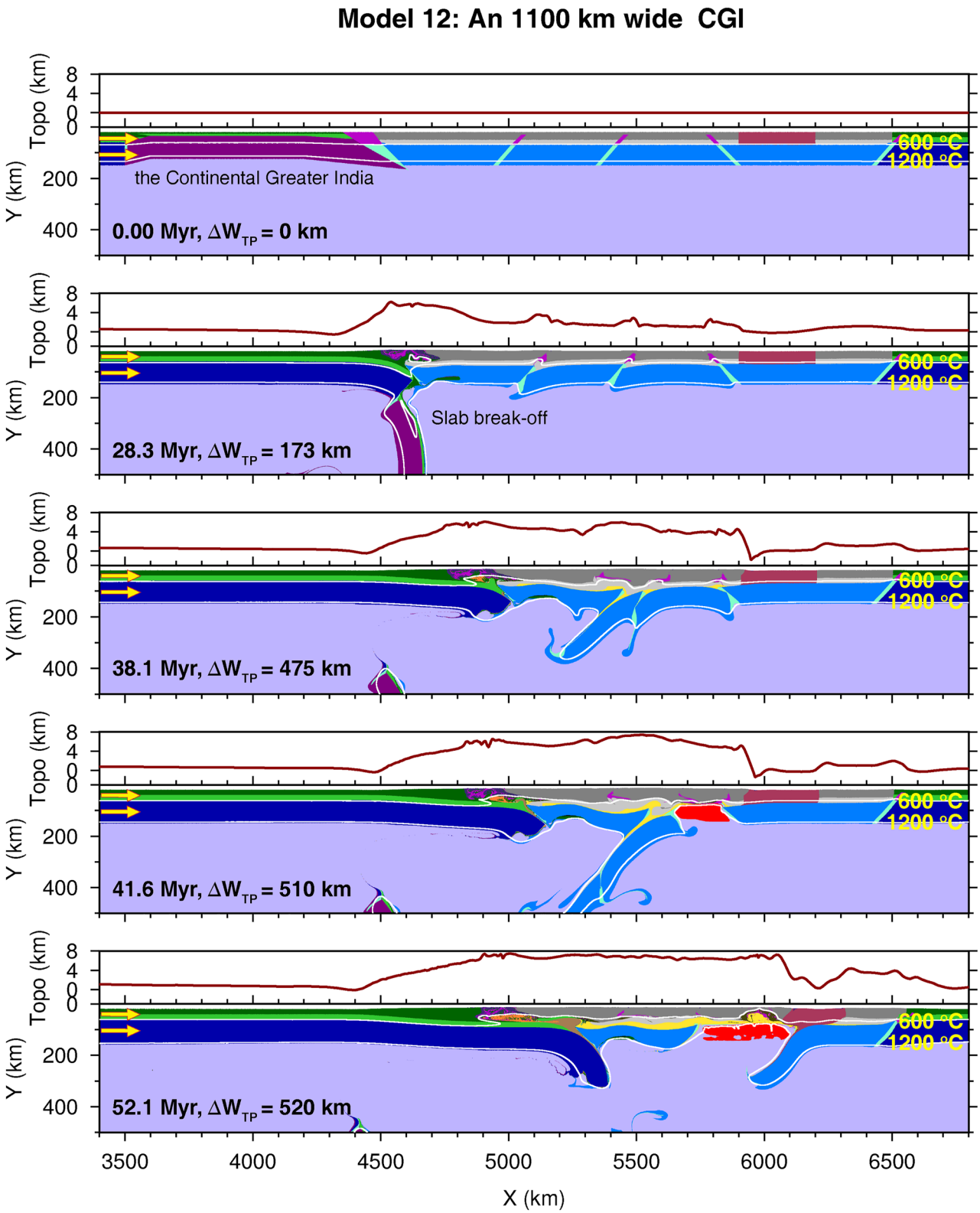

Figure 8. Simulation results of Model 12 with an 1,100 km wide terrane representing the Continental Greater India (CGI) between the Indian continent and Tibetan Plateau.

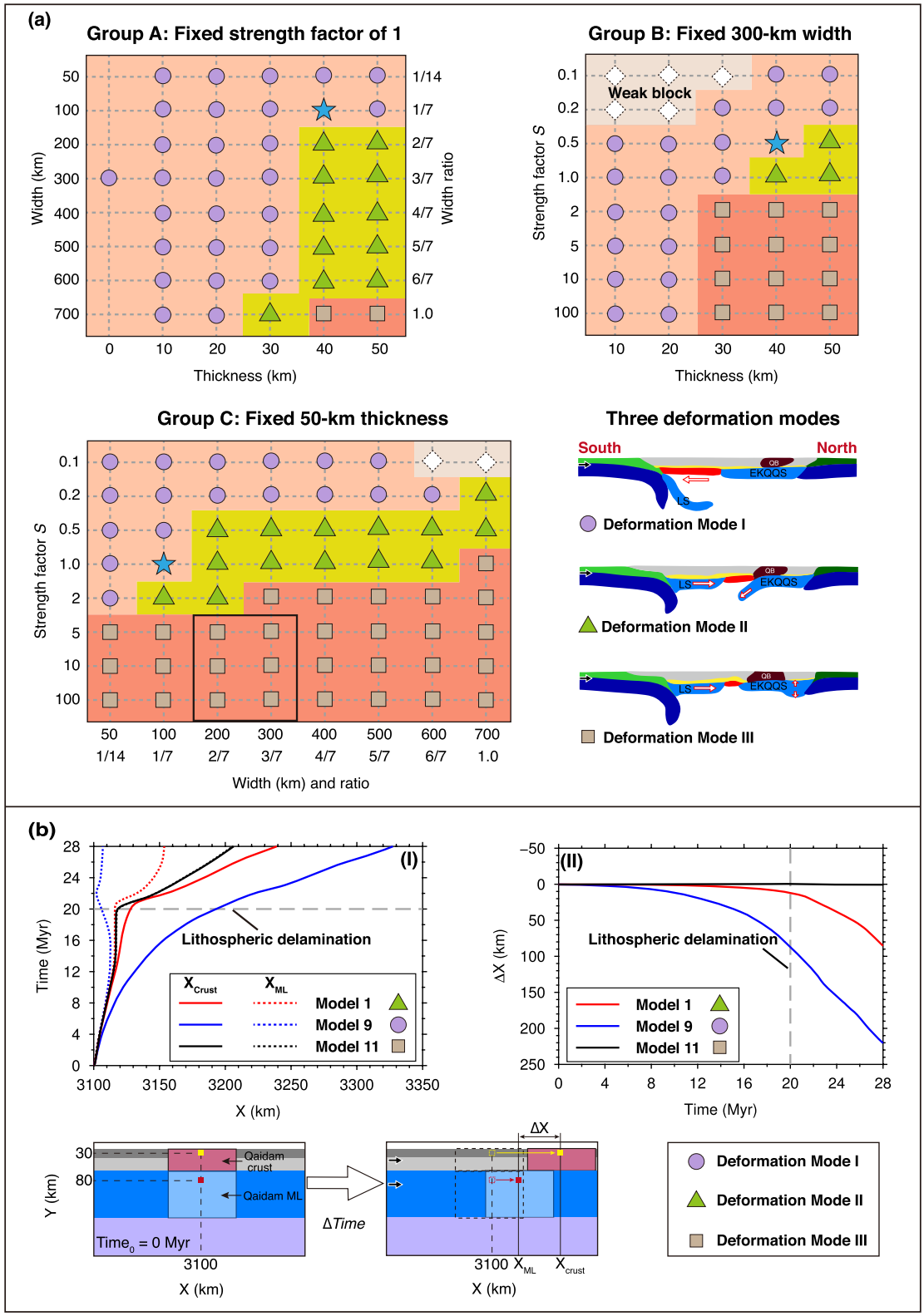

Figure 9.

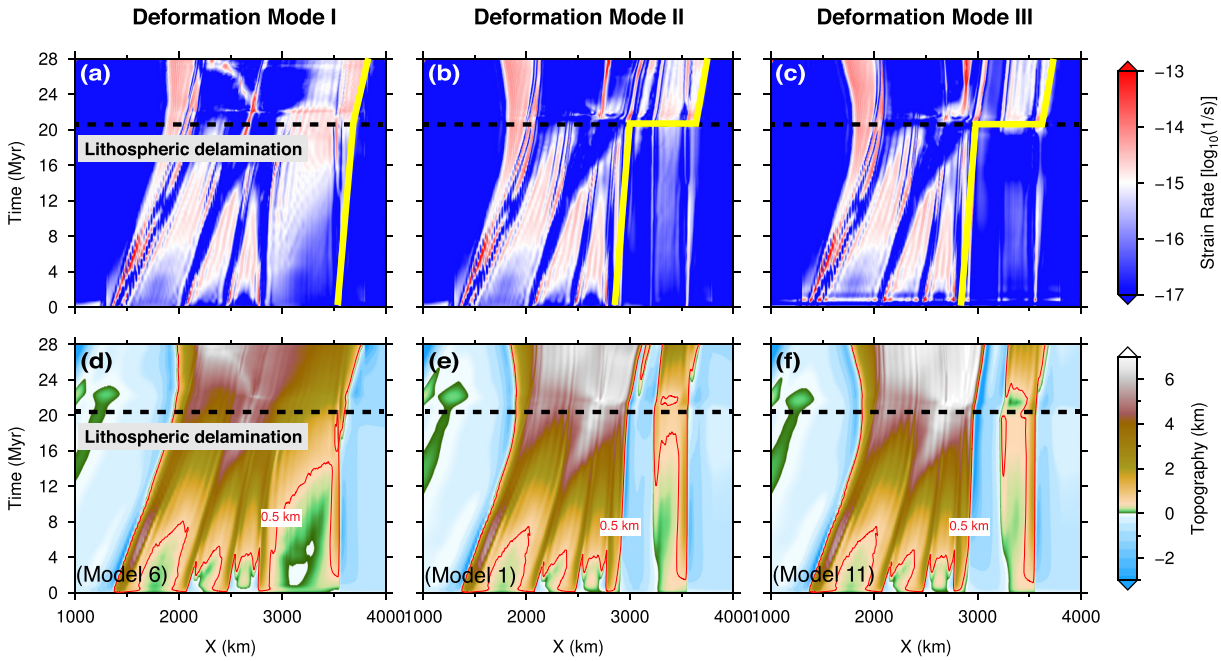

Figure 10. Evolution of crustal deformation and topography in different deformation modes. The left, middle and right columns represent the strain rate and topography in deformation Modes I, II and III, respectively. The upper row is the strain rate results and the lower row is the topography results. Black lines indicate the start time of the Songpan–Ganzi lithospheric delamination. Thick yellow lines point out the boundary of the strain rate.

Model 1 in Figure 9b-I). In this situation, the Qaidam crust can resist deformation in the early evolution of the model; however, after lithospheric delamination, the Qaidam crust and the partially molten asthenosphere is pushed northward, during which decoupling of the crust and mantle lithosphere takes placein the Qaidam region (Figures 3, 5b, 6a, 7b and 8). Coupling in the early stage of model evolution and decoupling in the later stage lead to flexing of the mantle lithosphere beneath the Qaidam region, which resembles southward subduction of the KQQ mantle lithosphere (e.g., Model 1 in Figures 9b-II). The third deformation mode (Deformation Mode III) is characterized by the northward-advancing Lhasa mantle lithosphere and a thickened mantle lithosphere north of the Qaidam region. If the Qaidam crust is very strong (i.e., a crustal strength factor >2), it has the capacity to resist deformation. A strong Qaidam crust couples with the underlying mantle lithosphere so that no relative horizontal displacement occurs between them throughout the model evolution (e.g., Model 11 in Figure 9b). After lithospheric delamination in northern Tibet, the Qaidam crust and the mantle lithosphere are pushed northward simultaneously, which results in lithospheric thickening north of the Qaidam region (Figure 7c). If there are more pre-existing weaknesses in the lithosphere north of the Qaidam crust, lithospheric thickening is more significant in this region (Figure S4a in Supporting Information S1). The deformation mode produced by an extremely wide Qaidam crust (700 km) is also similar to Deformation Mode III except that there is no lithospheric thickening in the north of the Qaidam region (Figure 5c).

Crustal deformation and topographic uplift have distinct responses in the three deformation modes. Crustal deformation and topographic uplift occur north of the Qaidam region soon after model initiation in all deformation

Figure 9. Lithospheric-deformation modes controlled by the relative displacement between the Qaidam crust and mantle lithosphere. (a) Three distinct lithospheric-deformation modes in different model groups with various Qaidam crustal widths, thicknesses and strength factors. Group A: Fixing the crustal strength factor as 1 and changing the crustal thicknesses and widths; Group B: Fixing the crustal width as 300 km and changing the crustal thicknesses and strength factors; Group C: Fixing the crustal thickness as 50 km and changing the crustal widths and strength factors. Purple circles represent Deformation Mode I; green triangles represent Deformation Mode II; brown squares represent Deformation Mode III; blue stars represent a transitional mode between Deformation Modes I and II and white diamonds indicate irregular deformation due to a weak Qaidam crust. (b) Evolution of the horizontal positions and relative horizontal displacement of the Qaidam crust and mantle lithosphere. In each evolutionary snapshot, the horizontal positions of Qaidam crust and mantle lithosphere are traced by markers inside the crust (the yellow marker in cartoon) and mantle lithosphere (the red marker in cartoon), respectively. (I) Evolution of the horizontal positions of the Qaidam crust and mantle lithosphere. Solid and dashed lines indicate the horizontal positions of the crust and mantle-lithosphere, respectively. The red, blue and black lines indicate results of Models 1, 9, and 11, respectively. ML: Mantle lithosphere. (II) Relative horizontal displacement between Qaidam crust and mantle lithosphere ($\Delta X = X_{crust} - X_{ML}$), which can approximately indicate the degrees of coupling of the Qaidam crust and mantle lithosphere. Similarly, the red, blue and black lines indicate the results of Models 1, 9, and 11, respectively.

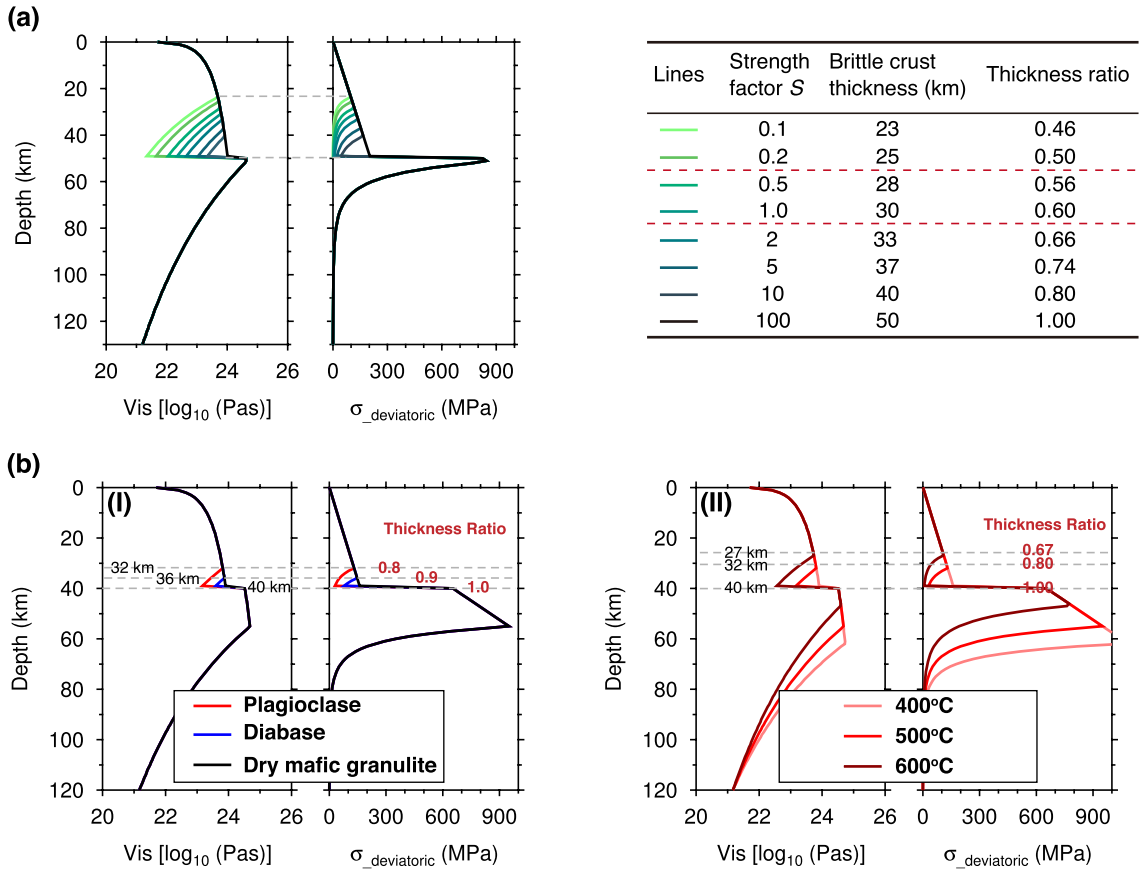

Figure 11. Initial strength of the Qaidam crust. (a) Initial crustal strength, brittle crustal layer thickness and ratio derived from different strength factors. (b) Estimated initial Qaidam crustal strength at the beginning of India-Aisa collision. (I) Crustal strength with different lower crustal compositions. The Moho temperature is assumed to be 500°C, and the lower crust is composed of plagioclase, diabase and dry mafic granulite, respectively. (II) Crustal strength with different Moho temperature. The lower crust is assumed to be composed of plagioclase, and the Moho temperature is 400°C, 500 and 600°C, respectively. Both in (I) and (II), the upper crust and mantle lithosphere are represented by wet quartz and dry olivine, respectively. Rheological parameters of different rocks are listed in Table 1. The strain rate is assumed to be 10^{-16} s^{-1}. The thickness ratios of the brittle crustal layer are all greater than 0.67 in (b), which corresponds to the crustal strength factor >2.

modes (Figures 10d–10f). In Deformation Mode I, crustal deformation and topographic uplift are distributed throughout the Tibetan domain, resulting in a unified plateau across Tibet (Figures 10a and 10d). But in Deformation Modes II and III, crustal deformation is concentrated mainly to the south of the Qaidam region, and only weak deformation exists to the north of the Qaidam region before lithospheric delamination (Figures 10b and 10c). If multiple lithospheric weak zones exist to the north of the Qaidam region, the crust would also deform intensively (Figure S4b in Supporting Information S1). After lithospheric delamination, crustal deformation transfers northward (Figures 10b and 10c). Finally, a primary plateau and a secondary orogen are developed to the south and north of the Qaidam region, respectively, and a basin is formed in Deformation Modes II and III (Figures 10e and 10f).

5.2. Lithospheric Deformation in Northeastern Tibet

Our model simulation results show that the initial width and strength of the Qaidam crust play important roles in controlling the deformation of the Tibetan lithosphere. Crustal strength can be reflected by the crustal thickness ratio of the strong brittle crustal layer in the entire crust, which is affected by the crustal strength factor. The larger the crustal strength factor, the thicker the strong brittle crustal layer and its thickness ratio, and the stronger the crust (Figure 11a). According to our simulations, for a medium width Qaidam crust, and if the crustal strength factor is less than 0.2, a thickness ratio of less than 0.50 is generated for the brittle crustal layer and the deformation is Mode I. If the crustal strength factor lies between 0.5 and 1, the thickness ratio of the strong brittle crustal layer will be between 0.56 and 0.60, and the deformation is Mode II. If the crustal strength factor is greater than 2,

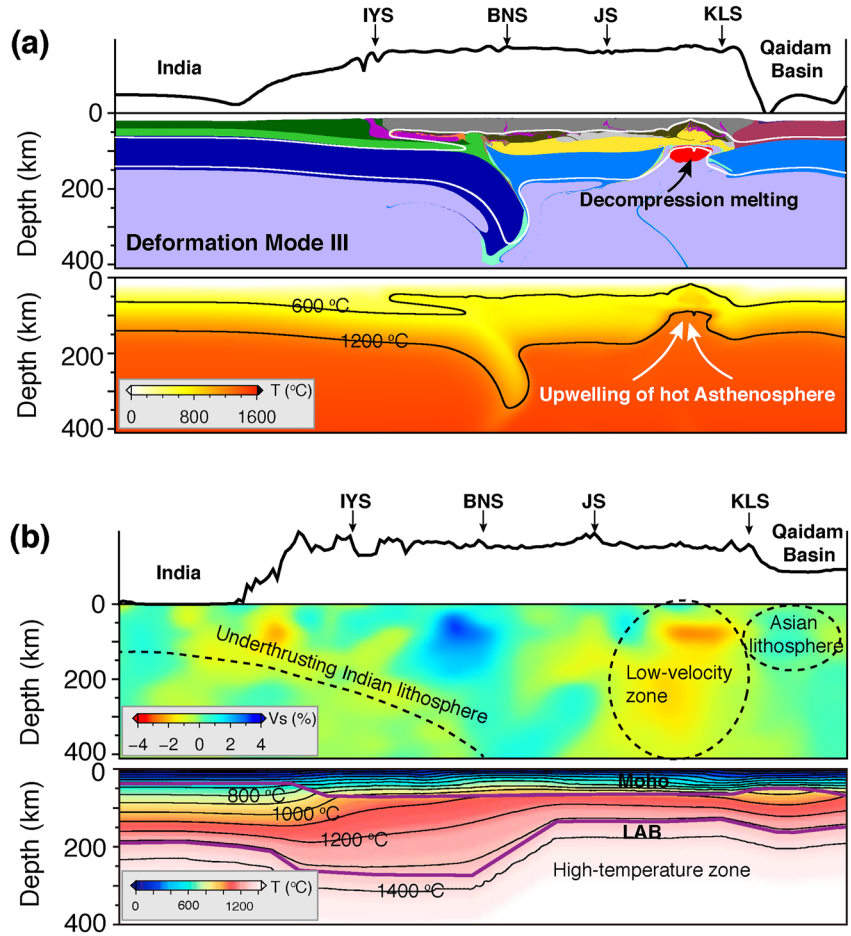

Figure 12. Comparisons of Deformation Mode III with observations. (a) Predicted topography, lithospheric structure and temperature field in Deformation Mode III. (b) Observed topography, shear wave velocity structure (Liang et al., 2012) and temperature distribution (modified from Tunini et al., 2016).

the thickness ratio of the strong brittle crustal layer will be greater than 0.66, and the deformation will be Mode III (see Group C in Figure 9a and the Table in Figure 11a). We can infer, therefore, that the type of the deformation mode in northeastern Tibet is determined by the Qaidam crustal width and strength. After taking the uncertainties of lower crustal compositions and Moho temperatures into account (details given in Text S3 in Supporting Information S1), we can estimate the initial thickness ratio of the brittle crustal layer to have been greater than 0.67 in the Qaidam Basin (Figure 11b), which according to our models implies that it was generated by a crustal strength factor greater than 2 (see the table in Figure 11a). Moreover, according to Yin and Harrison (2000) and Zuza et al. (2016), more than 300 km of Cenozoic crustal shortening occurred north of the Qaidam Basin. Combining that with the present-day 600 km width of northeastern Tibet, the initial width of northeastern Tibet was ~900 km. Thus, the ~300 km wide Qaidam Basin takes up about one third of the total initial width of northeastern Tibet. The Qaidam crust with an initial brittle crust thickness ratio of >0.67, a crustal strength factor >2, and an initial width ratio of ~1/3 would result in deformation Mode III, as outlined by the black rectangular area in Group C (Figure 9a).

Deformation under Mode III is also supported by many observations in Tibet. For instance, (a) the structure of the lithosphere under deformation Mode III is consistent with the P-wave velocity structure of the flat Asian lithosphere exposed in the mantle low-velocity zone (Figure 12); (b) upwelling of hot asthenosphere and decompression melting can explain the low mantle velocity zone beneath the Songpan–Ganzi terrane (Ceylan et al., 2012; Liang et al., 2012), and the high-temperature lithosphere and young potassic volcanism in the Songpan–Ganzi terranes (Barron & Priestley, 2009; Guo et al., 2006; Tunini et al., 2016); and (c) evidence of lithospheric thickening in northeastern Tibet is seen in receiver function results (Zhang et al., 2020). The deformation Mode III

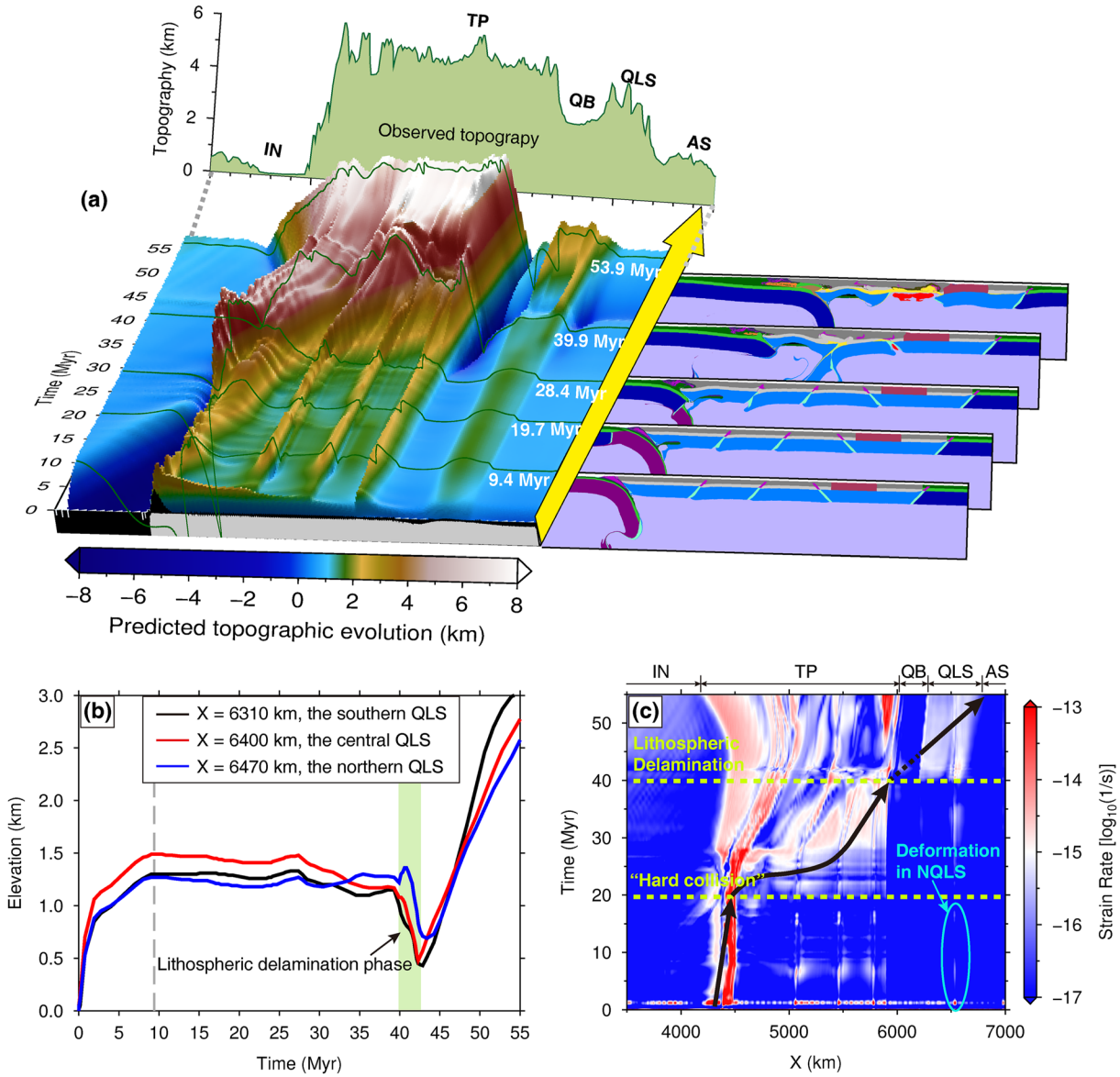

Figure 13. Predicted lithospheric deformation and topographic evolution in the Tibetan Plateau. (a) Composition and topography results of Model 13 containing an 1,100 km wide continental Greater India and a strong Qaidam crust whose crustal strength factor is 10. (b) Predicted topographic uplift of the Qilian Shan. Two phases of rapid topographic uplift occurred in the first 10 Myrs and later ~42–55 Myr. (c) Predicted crustal deformation of the Qilian Shan. Two phases of crustal deformation occurred in the Qilian Shan indicated by crustal strain rate results. In the first ~20 Myrs, the Qilian Shan appeared weak crustal deformation in the NQLS, but intense deformation immediately spread across the Qilian Shan after lithospheric delamination at ~40 Myr.

scenario also suggests that the Asian lithosphere did not subduct southward below the Songpan–Ganzi terrane, although the observed seismic results related to this are still debated (Ceylan et al., 2012; Kind et al., 2002; Liang et al., 2012; Yue et al., 2012; Zhao et al., 2011). Our results provide independent evidence from a geodynamic point of view for this debate.

5.3. Crustal Deformation and Topographic Evolution in Northeastern Tibet

In deformation Mode III, our simulations obtain a flat-topped plateau in the south, an intermontane basin in the middle, and a secondary highland in the north, which is similar to the general topography of Tibet to the south and north of the Qaidam Basin (Figure 10f). The Model 13 which contains an 1,100 km wide Continental Greater India and a strong Qaidam crust with crustal strength factor of 10, can evolve to ~55 Myr and produce similar

lithospheric structure and topography to deformation Mode III (Figure 13). Here, we emphatically discuss the topographic evolution and lithospheric deformation in the Qilian Shan.

According to the simulation results of Model 13, the Qilian Shan gains an elevation of ~1.5 km in 10 Myrs after initiation of the model (Figures 13a and 13b). The elevation in the Qilian Shan is maintained ~1.0–1.5 km over a long period of time, but rapidly decreases to ~0.5 km during the lithospheric delamination of the Qiangtang and Songpan-Ganzi terranes (Figure 13b). After that, the elevation rapidly uplifts again to ~3.0 km. The topographic responses are consistent with the features of crustal deformation, as revealed by the strain rate results which show weak but durable crustal deformation in the weak NQLS in the early stage of model evolution and intense crustal deformation across the Qilian Shan soon after lithospheric delamination (Figure 13c). If the Qilian Shan terrane is divided further into three sub-blocks—or if it contains more weak zones, topographic uplift and crustal deformation are more intense in this region (Figures S4 and S5 in Supporting Information S1).

The two phases of crustal deformation and surface uplift in our models are consistent with observations from northeastern Tibet, where extensive crustal deformation occurred in the Eocene–Oligocene and from the Miocene to the present (Figure 1). Early crustal deformation occurred mainly around the Qaidam Basin (Figure 1), where the Altyn Tagh fault, Kunlun fault, and Qimen Tagh faults became active from 49 Ma to 35 Ma, and the North Qaidam thrust systems was active at 65–50 Ma (Clark et al., 2010; Jolivet et al., 2001; Yin et al., 2008). Crustal shortening also occurred in the hinterland and on the northern margin of the Qilian Shan at ca. ~55 Ma, along with surface uplift (Qi et al., 2016; Zuza et al., 2019), and the Nan Shan thrust belt in central Qilian Shan was shortened at 33 Ma (Yin et al., 2002). The West Qinling thrust started deforming ca. ~50 Ma in response to the India–Asia collision, causing uplift of ~0.8 km during 50–30 Ma, which is approximately consistent with the early ~1.0–1.5 km elevation predicted in our simulations (Clark et al., 2010). Likewise, the clockwise rotation of the crust in the Xining–Lanzhou region (beginning at ca. 45 Ma) indicates early crustal deformation in this region (Dupont–Nivet et al., 2004). Early crustal thickening produced considerable topographic relief in northeastern Tibet, as indicated by the appearance of conifers in the Xining Basin at 38 Ma that required high-altitude climatic conditions (Dupont–Nivet et al., 2008). Since the Miocene, new large-scale crustal deformation has taken place in northeastern Tibet (Figure 1). The Eastern Kunlun fault, the southern boundary of northeastern Tibet, was activated at ca. 20 Ma, and the North Qilian Shan and Haiyuan faults along the northern margin experienced rapid exhumation at 10–8 Ma (Duvall et al., 2013). Other faults and basins between the southern and northern margins underwent deformation during this phase, including the Jishi Shan fault at 13 Ma, the Laji Shan fault at 22 Ma, the Elashan fault at 13 Ma, the Wenquan fault at 9 Ma, the Jiuxi Basin at 13–10 Ma, and the Guide Basin at 17 Ma (Duvall et al., 2013 and references therein; Wang et al., 2016). Extensive crustal deformation caused northeastern Tibet to expand rapidly eastward toward the Liupan Shan fault at 8 Ma, and to thicken to 55–60 km causing uplift to ~4 km (Li et al., 2014; Zheng et al., 2006).

Based on the aforementioned observations, two contrasting views have been proposed to address crustal deformation in northeastern Tibet: (a) plateau formation occurred nearly synchronously across the northern and southern margins of Tibet since the onset of the India–Asia collision (Dupont–Nivet et al., 2004; Yin et al., 2002); (b) plateau has been developed progressively northward and it reached the northeastern Tibet at 20–15 Ma (e.g., England & Houseman, 1986; Meyer et al., 1998; Tapponnier et al., 2001). However, these two views cannot be reconciled with the multi-phase Cenozoic deformation in northeastern Tibet. Recently, Wang et al. (2022) proposed a multi-stage lithospheric delamination model to explain the pulsed uplift events in northeastern Tibet at 30 Ma and 10 Ma. But this model does not explain the Cenozoic deformation before 30 Ma. Our simulations replicate the two phases of crustal deformation in the Qilian Shan in the early and late stages of the model initiation, and the simulations provide the following plausible explanations of the crustal growth in northeastern Tibet. The strong Qaidam Basin caused stress to transfer rapidly to northeastern Tibet shortly after the India–Asia collision (Bian et al., 2020; Dayem et al., 2009), which activated pre-existing weaknesses (e.g., sutures and faults) to produce early crustal shortening and surface uplift in the Eocene to Oligocene (Figure 13c and Figure S5a in Supporting Information S1). As the Indian continent advanced northward, the mantle lithosphere in central and northern Tibet was thinned by delamination or convection removal in the Miocene (Molnar et al., 1993), which decreased the strength of the Tibetan lithosphere. From the Miocene, the strong Qaidam crust, coupled with the underlying mantle lithosphere, was pushed rapidly northward owing to a change in the lithospheric structure of central and northern Tibet. The advance of the Qaidam Basin thickened the Qilian Shan lithosphere, producing the second wave of large-scale crustal deformation and topographic uplift (Figure 13 and Figure S5 in Supporting Information S1). Two phases of strong tectonic compressional stress in the northern Qaidam margin at 52–45 Ma

and 21–15 Ma provide strong support for our explanations (Sun et al., 2022). The active left-slip Altyn Tagh fault with ~360–470 km offset in the west of the Qaidam Basin recorded the northeastward movement of the basin (Cheng et al., 2016; Yin et al., 2002).

5.4. Comparison With Early Geodynamic Modeling Work

Previous numerical modeling works about the India-Asia collision mostly regarded the Tibetan lithosphere as a homogeneous block (Capitanio & Replumaz, 2013; Li et al., 2016; Pusok & Kaus, 2015), but lithospheric heterogeneities have been gaining more attention in recent years. For example, Huangfu et al. (2018) divided the Tibetan lithosphere into a strong block in south Tibet and a weak block in north Tibet to simulate different lithospheric delamination styles in western and eastern Tibet; Kelly et al. (2020) considered the inherited lithospheric heterogeneities of each terranes in their models to study the post-collisional Himalayan-Tibetan evolution; Kong et al. (1997) and Chen et al. (2020) evaluated the role of the pre-existing weak suture zones inside Tibet on the formation of the Tibetan Plateau; and Zhang et al. (2022) explored the topographic response of the local basin basements inside the Tibet. These numerical simulations further advanced our understanding about the geodynamic processes of the Tibetan Plateau, but none of them specifically focused on lithospheric deformation in northeastern Tibet.

Our numerical models referred to the multi-terrane structure of the Tibetan lithosphere, and simultaneously took local weak sutures and strong Qaidam basement into account. We emphatically studied how the strong Qaidam Basin affected lithospheric deformation in northeastern Tibet. As suggested by Bian et al. (2020), the strong Qaidam Basin facilitated stress propagation to activate pre-existing weak zones in northeastern Tibet, causing diachronous uplift in Qilian Shan in the early India-Asia collision. The instant distal deformation is also related to the strength of the Tibetan lithosphere, a very strong Tibetan lithosphere would not produce distal deformation in northeastern Tibet (Huangfu et al., 2022). Finally, the strong basement developed into the Qaidam Basin, and the weak Qilian Shan became a part of the Tibetan Plateau (Sun & Liu, 2018). Our simulation results also showed lithospheric delamination in northern Tibet and lithospheric thickening in northeastern Tibet, and the two dynamic processes were connected by the strong Qaidam Basin. Compared with the 3-D models in Chen et al. (2020) and Zhang et al. (2022), our 2-D models were unable to reproduce along-strike deformation and lateral expansion in northeastern Tibet.

6. Model Limitations

Our simulation results can help us to a certain extent to understand the role of the stronger Qaidam lithosphere in the deformation of northeastern Tibet. Some simplifications are necessary in our numerical models, but perhaps also affect our simulation results, for example,: (a) The dipping directions of the sutures greatly affecting the deformation of Tibetan lithosphere are hard to confirm, and we only referred to the most–likely combination of the sutures and did not take other possibilities into account. (b) The India–Asia convergence rate varied with time, and it decreased from ~10 to 11 cm/yr at ca. 60 Ma to ~3–4 cm/yr at ca. 10 Ma (Cande et al., 2010; Molnar & Stock, 2009). To simplify this process, we simply used a constant convergence rate of 4 cm/yr in our 2-D models. Such simplification led to a trade-off between the evolution time and the width of the Continental Greater India. Undoubtedly, the convergence rate is a crucial factor affecting the deformation of orogens (Li et al., 2013; Vogt et al., 2017), and its impact on the Tibetan Plateau needs more in-depth and detailed research.

Furthermore, addition of the Continental Greater India can extend model evolution to 52–55 Myr, which is consistent with India-Asia collision duration of ~56 Myr (Hu et al., 2016). The extended model evolution also makes some lithospheric deformation more time-matched with observations (Figure 13), such as (a) the delamination of the Songpan-Ganzi lithosphere at ~40 Myr is consistent with the Mid-Miocene potassic volcanic rocks in north Tibet (Chung et al., 2005); and (b) two phases of crustal deformation in Qilian Shan in 0–10 and 42–55 Myr are also consistent with the two-stage crustal deformation during the Eocene–Oligocene and since the Miocene in northeastern Tibet (Figure 1; Duvall et al., 2013). However, in our models, subduction of the Continental Greater India absorbs most of early convergence, during which only local lithospheric deformation and topographic uplift occur in the subduction zone and weak sutures. Undeniably, such lithospheric deformation does not match well with all the observations in the Himalayan-Tibetan orogenic system, for example, the regional-differentiation uplift history of the Himalaya-Tibetan plateau (Ding et al., 2022), substantial Eocene (ultra) potassic and adakitic

igneous rocks in central Tibet (Chung et al., 2005; Kapp & DeCelles, 2019) and widespread Eocene–Oligocene fold-thrust belt from the Himalaya to Qilian Shan (Li et al., 2015). The main cause for these differences is that our models do not distinguish the inherited lithospheric heterogeneities of each terrane in the Tibetan lithosphere like models in Kelly et al. (2020).

At last, the Qaidam Block was squeezed to the northeast of the Tarim Block by the Indian collision in the Cenozoic (Meng et al., 2008), and during this period, the Tarim Block rapidly concentrated the strain along its southern margin and restrained the northward propagation of deformation (Dayem et al., 2009). Therefore, deformation in the Qaidam region was shielded to some extent by the adjoining Tarim region. However, our 2-D models are incapable of simulating the effects of out-of-plane motion and deformation.

7. Conclusions

We used high-resolution 2-D thermal-mechanical simulations to assess the effects of Qaidam crustal structures and strength on the deformation history of northeastern Tibet during the Cenozoic India-Asia collision. All simulations predict lithospheric delamination and mantle decompression melting in northern Tibet, but varying the width, thickness, and strength of the Qaidam crust leads to three end-member scenarios for the first-order Tibetan lithospheric deformation: (a) southward delamination of the Lhasa mantle lithosphere and an almost undeformed mantle lithosphere beneath the Eastern Kunlun-Qaidam terrane and the Qilian Shan thrust belt (Deformation Mode I), (b) ongoing northward-advancing Lhasa mantle lithosphere and southward subduction of the mantle lithosphere beneath the Eastern Kunlun-Qaidam terrane and the Qilian Shan thrust belt (Deformation Mode II), and (c) ongoing northward-moving Lhasa mantle lithosphere and thickened lithosphere to the north of the Qaidam Basin (deformation Mode III). Different degrees of coupling of the crust and mantle lithosphere in the Qaidam Basin may contribute to distinct deformation modes. After estimating the initial Qaidam crustal width and strength, and comparing them with the tested Qaidam crustal parameters, we infer that the lithospheric deformation in northeastern Tibet is consistent with Deformation Mode III. This inference is supported by many observations in Tibet. Two phases of crustal deformation and topographic uplift north of the Qaidam Basin are replicated in our models. The first phase of crustal deformation results from the activation of pre-existing weaknesses shortly after the onset of the India–Asia collision, and this deformation is sustained for an extended period. The second phase of crustal deformation is induced by lithospheric delamination in northern Tibet. Our results consistent with observations provide a plausible explanation for the tectonic history of northeastern Tibet.

Data Availability Statement

All simulation results are available at https://zenodo.org/record/7542591.

Acknowledgments
The authors sincerely thank Prof. Taras Gerya for providing the I2VIS package used in this study. The authors also thank Prof. Yingjie Yang and Xiaofeng Liang for kindly providing the Vs model of the Tibetan lithosphere, Dr. Zhiyong Yan for drawing the cartoons shown in Figure 8a, and Dr. Lipeng He for suggestions for the improvement of our figures. The authors acknowledge that all the figures used in this work were prepared with the Generic Mapping Tools (GMT, http://www.soest.hawaii.edu/gmt/). This study was supported by the National Key R&D Program of China (2022YFF0800800) and the National Natural Science Foundation of China (Grants 41974110, 41731072, 41890814). The simulations were executed on the TianHe-1A system at the National Supercomputer Center in Tianjin, the Beijing Super Cloud Computing Center, and Supercomputing Laboratory at IGGCAS. The authors are very grateful to the constructive comments provided by two anonymous reviewers and Prof. Chris Beaumont, which significantly improved the presentation of our work.

References

Barron, J., & Priestley, K. (2009). Observations of frequency-dependent Sn propagation in northern Tibet. *Geophysical Journal International*, *179*(1), 475–488. https://doi.org/10.1111/j.1365-246X.2009.04318.x

Beaumont, C., Jamieson, R. A., Butler, J. P., & Warren, C. J. (2009). Crustal structure: A key constraint on the mechanism of ultra-high-pressure rock exhumation. *Earth and Planetary Science Letters*, *287*(1–2), 116–129. https://doi.org/10.1016/j.epsl.2009.08.001

Bian, S., Gong, J., Chen, L., Zuza, A. V., Chen, H., Lin, X., et al. (2020). Diachronous uplift in intra-continental orogeny: 2D thermo-mechanical modeling of the India-Asia collision. *Tectonophysics*, *775*, 228310. https://doi.org/10.1016/j.tecto.2019.228310

Bittner, D., & Schmeling, H. (1995). Numerical modelling of melting processes and induced diapirism in the lower crust. *Geophysical Journal International*, *123*(1), 59–70. https://doi.org/10.1111/j.1365-246X.1995.tb06661.x

Cande, S. C., Patriat, P., & Dyment, J. (2010). Motion between the Indian, Antarctic and African plates in the early Cenozoic. *Geophysical Journal International*, *183*(1), 127–149. https://doi.org/10.1111/j.1365-246X.2010.04737.x

Capitanio, F. A., & Replumaz, A. (2013). Subduction and slab breakoff controls on Asian indentation tectonics and Himalayan Western syntaxis formation. *Geochemistry, Geophysics, Geosystems*, *14*(9), 3515–3531. https://doi.org/10.1002/ggge.20171

Ceylan, S., Ni, J., Chen, J. Y., Zhang, Q., Tilmann, F., & Sandvol, E. (2012). Fragmented Indian plate and vertically coherent deformation beneath eastern Tibet. *Journal of Geophysical Research*, *117*(B11). https://doi.org/10.1029/2012JB009210

Chen, B., Liu, J., Chen, C., Du, J., & Sun, Y. (2015). Elastic thickness of the Himalayan–Tibetan orogen estimated from the fan wavelet coherence method, and its implications for lithospheric structure. *Earth and Planetary Science Letters*, *409*, 1–14. https://doi.org/10.1016/j.epsl.2014.10.039

Chen, L., Capitanio, F. A., Liu, L., & Gerya, T. V. (2017). Crustal rheology controls on the Tibetan plateau formation during India-Asia convergence. *Nature Communications*, *8*(1), 1–8. https://doi.org/10.1038/ncomms15992

Chen, L., Liu, L., Capitanio, F. A., Gerya, T. V., & Li, Y. (2020). The role of pre-existing weak zones in the formation of the Himalaya and Tibetan plateau: 3-D thermomechanical modelling. *Geophysical Journal International*, *221*(3), 1971–1983. https://doi.org/10.1093/gji/ggaa125

Cheng, F., Jolivet, M., Fu, S., Zhang, C., Zhang, Q., & Guo, Z. (2016). Large-scale displacement along the Altyn Tagh fault (north Tibet) since its Eocene initiation: Insight from detrital zircon U–Pb geochronology and subsurface data. *Tectonophysics*, *677*, 261–279. https://doi.org/10.1016/j.tecto.2016.04.023

Cheng, F., Jolivet, M., Guo, Z., Wang, L., Zhang, C., & Li, X. (2021). Cenozoic evolution of the Qaidam basin and implications for the growth of the northern Tibetan plateau: A review. *Earth-Science Reviews*, *220*, 103730. https://doi.org/10.1016/j.earscirev.2021.103730

Chung, S. L., Chu, M. F., Zhang, Y., Xie, Y., Lo, C. H., Lee, T. Y., et al. (2005). Tibetan tectonic evolution inferred from spatial and temporal variations in post-collisional magmatism. *Earth-Science Reviews*, *68*(3–4), 173–196. https://doi.org/10.1016/j.earscirev.2004.05.001

Clark, M. K., Farley, K. A., Zheng, D., Wang, Z., & Duvall, A. R. (2010). Early Cenozoic faulting of the northern Tibetan Plateau margin from apatite (U–Th)/He ages. *Earth and Planetary Science Letters*, *296*(1–2), 78–88. https://doi.org/10.1016/j.epsl.2010.04.051

Clark, M. K., & Royden, L. H. (2000). Topographic ooze: Building the eastern margin of Tibet by lower crustal flow. *Geology*, *28*(8), 703–706. https://doi.org/10.1130/0091-7613(2000)28<703:TOBTEM>2.0.CO;2

Clauser, C., & Huenges, E. (1995). Thermal conductivity of rocks and minerals. In T. J. Ahrens (Ed.), *Rock physics and phase relations AGU Ref. shelf* (pp. 105–126). AGU.

Crameri, F., Schmeling, H., Golabek, G. J., Duretz, T., Orendt, R., Buiter, S. J. H., et al. (2012). A comparison of numerical surface topography calculations in geodynamic modelling: An evaluation of the 'sticky air' method. *Geophysical Journal International*, *189*(1), 38–54. https://doi.org/10.1111/j.1365-246X.2012.05388.x

Dayem, K. E., Molnar, P., Clark, M. K., & Houseman, G. A. (2009). Far-field lithospheric deformation in Tibet during continental collision. *Tectonics*, *28*(6). https://doi.org/10.1029/2008TC002344

Deng, Y., & Tesauro, M. (2016). Lithospheric strength variations in Mainland China: Tectonic implications. *Tectonics*, *35*(10), 2313–2333. https://doi.org/10.1002/2016TC004272

Ding, L., Kapp, P., Cai, F., Garzione, C. N., Xiong, Z., Wang, H., & Wang, C. (2022). Timing and mechanisms of Tibetan Plateau uplift. *Nature Reviews Earth and Environment*, *3*(10), 1–16. https://doi.org/10.1038/s43017-022-00318-4

Dupont-Nivet, G., Hoorn, C., & Konert, M. (2008). Tibetan uplift prior to the Eocene-Oligocene climate transition: Evidence from pollen analysis of the Xining Basin. *Geology*, *36*(12), 987–990. https://doi.org/10.1130/G25063A.1

Dupont-Nivet, G., Horton, B. K., Butler, R. F., Wang, J., Zhou, J., & Waanders, G. L. (2004). Paleogene clockwise tectonic rotation of the Xining-Lanzhou region, northeastern Tibetan Plateau. *Journal of Geophysical Research*, *109*(B4). https://doi.org/10.1029/2003JB002620

Duvall, A. R., Clark, M. K., Kirby, E., Farley, K. A., Craddock, W. H., Li, C., & Yuan, D. Y. (2013). Low-temperature thermochronometry along the Kunlun and Haiyuan Faults, NE Tibetan Plateau: Evidence for kinematic change during late-stage orogenesis. *Tectonics*, *32*(5), 1190–1211. https://doi.org/10.1002/tect.20072

England, P., & Houseman, G. (1986). Finite strain calculations of continental deformation: 2. Comparison with the India-Asia collision zone. *Journal of Geophysical Research*, *91*(B3), 3664–3676. https://doi.org/10.1029/JB091iB03p03664

Gerya, T. (2011). *Introduction to numerical geodynamic modelling*. Cambridge University Press.

Gerya, T. V., & Yuen, D. A. (2003a). Characteristics-based marker-in-cell method with conservative finite-differences schemes for modeling geological flows with strongly variable transport properties. *Physics of the Earth and Planetary Interiors*, *140*(4), 293–318. https://doi.org/10.1016/j.pepi.2003.09.006

Goussin, F., Riel, N., Cordier, C., Guillot, S., Boulvais, P., Roperch, P., et al. (2020). Carbonated inheritance in the Eastern Tibetan lithospheric mantle: Petrological evidences and geodynamic implications. *Geochemistry, Geophysics, Geosystems*, *21*(2), e2019GC008495. https://doi.org/10.1029/2019GC008495

Guillot, S., Garzanti, E., Baratoux, D., Marquer, D., Mahéo, G., & de Sigoyer, J. (2003). Reconstructing the total shortening history of the NW Himalaya. *Geochemistry, Geophysics, Geosystems*, *4*(7). https://doi.org/10.1029/2002GC000484

Guo, Z., Wilson, M., Liu, J., & Mao, Q. (2006). Post-collisional, potassic and ultrapotassic magmatism of the northern Tibetan Plateau: Constraints on characteristics of the mantle source, geodynamic setting and uplift mechanisms. *Journal of Petrology*, *47*(6), 1177–1220. https://doi.org/10.1093/petrology/egl007

Heron, P. J., Pysklywec, R. N., & Stephenson, R. (2016). Lasting mantle scars lead to perennial plate tectonics. *Nature Communications*, *7*(1), 1–7. https://doi.org/10.1038/ncomms11834

Hu, X., Garzanti, E., Wang, J., Huang, W., An, W., & Webb, A. (2016). The timing of India-Asia collision onset–Facts, theories, controversies. *Earth-Science Reviews*, *160*, 264–299. https://doi.org/10.1016/j.earscirev.2016.07.014

Huangfu, P., Li, Z. H., Fan, W., Zhang, K. J., & Shi, Y. (2022). Contrasting collision-induced far-field orogenesis controlled by thermo-rheological properties of the composite terrane. *Gondwana Research*, *103*, 404–423. https://doi.org/10.1016/j.gr.2021.10.020

Huangfu, P., Li, Z. H., Gerya, T., Fan, W., Zhang, K. J., Zhang, H., & Shi, Y. (2018). Multi-terrane structure controls the contrasting lithospheric evolution beneath the Western and central–eastern Tibetan plateau. *Nature Communications*, *9*(1), 1–11. https://doi.org/10.1038/s41467-018-06233-x

Ingalls, M., Rowley, D. B., Currie, B., & Colman, A. S. (2016). Large-scale subduction of continental crust implied by India–Asia mass-balance calculation. *Nature Geoscience*, *9*(11), 848–853. https://doi.org/10.1038/ngeo2806

Jolivet, M., Brunel, M., Seward, D., Xu, Z., Yang, J., Roger, F., et al. (2001). Mesozoic and Cenozoic tectonics of the northern edge of the Tibetan plateau: Fission-track constraints. *Tectonophysics*, *343*(1–2), 111–134. https://doi.org/10.1016/S0040-1951(01)00196-2

Kapp, P., & DeCelles, P. G. (2019). Mesozoic–Cenozoic geological evolution of the Himalayan-Tibetan orogen and working tectonic hypotheses. *American Journal of Science*, *319*(3), 159–254. https://doi.org/10.2475/03.2019.01

Karato, S., Paterson, M. S., & Fitzgerald, J. D. (1986). Rheology of synthetic olivine aggregates: Influence of grain size and water. *Journal of Geophysical Research*, *91*(B8), 8151–8176. https://doi.org/10.1029/JB091iB08p08151

Karplus, M. S., Zhao, W., Klemperer, S. L., Wu, Z., Mechie, J., Shi, D., et al. (2011). Injection of Tibetan crust beneath the south Qaidam Basin: Evidence from INDEPTH IV wide-angle seismic data. *Journal of Geophysical Research*, *116*(B7), B07301. https://doi.org/10.1029/2010JB007911

Kelly, S., Beaumont, C., & Butler, J. P. (2020). Inherited terrane properties explain enigmatic post-collisional Himalayan-Tibetan evolution. *Geology*, *48*(1), 8–14. https://doi.org/10.1130/G46701.1

Kind, R., Yuan, X., Saul, J., Nelson, D., Sobolev, S. V., Mechie, J., et al. (2002). Seismic images of crust and upper mantle beneath Tibet: Evidence for Eurasian plate subduction. *Science*, *298*(5596), 1219–1221. https://doi.org/10.1126/science.1078115

Kong, X., Yin, A., & Harrison, T. M. (1997). Evaluating the role of preexisting weaknesses and topographic distributions in the Indo-Asian collision by use of a thin-shell numerical model. *Geology*, *25*(6), 527–530. https://doi.org/10.1130/0091-7613(1997)025<0527:ETROPW>2.3.CO;2

Li, H., Shen, Y., Huang, Z., Li, X., Gong, M., Shi, D., et al. (2014). The distribution of the mid-to-lower crustal low-velocity zone beneath the northeastern Tibetan Plateau revealed from ambient noise tomography. *Journal of Geophysical Research: Solid Earth*, *119*(3), 1954–1970. https://doi.org/10.1002/2013JB010374

Li, Y., Wang, C., Dai, J., Xu, G., Hou, Y., & Li, X. (2015). Propagation of the deformation and growth of the Tibetan–Himalayan orogen: A review. *Earth-Science Reviews*, *143*, 36–61. https://doi.org/10.1016/j.earscirev.2015.01.001

Li, Z. H., Liu, M., & Gerya, T. (2016). Lithosphere delamination in continental collisional orogens: A systematic numerical study. *Journal of Geophysical Research: Solid Earth*, *121*(7), 5186–5211. https://doi.org/10.1002/2016JB013106

Li, Z. H., Xu, Z., Gerya, T., & Burg, J. P. (2013). Collision of continental corner from 3-D numerical modeling. *Earth and Planetary Science Letters*, *380*, 98–111. https://doi.org/10.1016/j.epsl.2013.08.034

Liang, X., Sandvol, E., Chen, Y. J., Hearn, T., Ni, J., Klemperer, S., et al. (2012). A complex Tibetan upper mantle: A fragmented Indian slab and no south-verging subduction of Eurasian lithosphere. *Earth and Planetary Science Letters*, *333*, 101–111. https://doi.org/10.1016/j.epsl.2012.03.036

Litasov, K. D., Shatskiy, A., Ohtani, E., & Katsura, T. (2011). Systematic study of hydrogen incorporation into Fe-free wadsleyite. *Physics and Chemistry of Minerals*, *38*(1), 75–84. https://doi.org/10.1007/s00269-010-0382-3

Ma, L., Wang, Q., Kerr, A. C., & Tang, G. J. (2021). Nature of the pre-collisional lithospheric mantle in central Tibet: Insights to Tibetan Plateau uplift. *Lithos*, *388*, 106076. https://doi.org/10.1016/j.lithos.2021.106076

Meng, J., Wang, C., Zhao, X., Coe, R., Li, Y., & Finn, D. (2012). India-Asia collision was at 24 N and 50 Ma: Palaeomagnetic proof from southernmost Asia. *Scientific Reports*, *2*(1), 1–11. https://doi.org/10.1038/srep00925

Meng, Q. R., Fang, X., Burchfiel, B. C., & Wang, E. (2008). Cenozoic tectonic development of the Qaidam Basin in the northeastern Tibetan Plateau. Investigations into the tectonics of the Tibetan Plateau. *Geological Society of America Special Paper*, *444*, 1–24.

Meyer, B., Tapponnier, P., Bourjot, L., Metivier, F., Gaudemer, Y., Peltzer, G., et al. (1998). Crustal thickening in Gansu-Qinghai, lithospheric mantle subduction, and oblique, strike-slip controlled growth of the Tibet plateau. *Geophysical Journal International*, *135*(1), 1–47. https://doi.org/10.1046/j.1365-246X.1998.00567.x

Molnar, P., England, P., & Martinod, J. (1993). Mantle dynamics, uplift of the Tibetan Plateau, and the Indian monsoon. *Reviews of Geophysics*, *31*(4), 357–396. https://doi.org/10.1029/93RG02030

Molnar, P., & Stock, J. M. (2009). Slowing of India's convergence with Eurasia since 20 Ma and its implications for Tibetan mantle dynamics. *Tectonics*, *28*(3). https://doi.org/10.1029/2008TC002271

Murphy, M. A., Yin, A., Harrison, T. M., Durr, S. B., Ryerson, F. J., Kidd, W. S. F., et al. (1997). Did the Indo-Asian collision alone create the Tibetan plateau? *Geology*, *25*(8), 719–722. https://doi.org/10.1130/0091-7613(1997)025<0719:DTIACA>2.3.CO;2

O'Reilly, S. Y., & Griffin, W. L. (2013). Mantle metasomatism. In *Metasomatism and the chemical transformation of rock* (pp. 471–533). Springer. https://doi.org/10.1007/978-3-642-28394-9_12

Pusok, A. E., & Kaus, B. J. (2015). Development of topography in 3-D continental-collision models. *Geochemistry, Geophysics, Geosystems*, *16*(5), 1378–1400. https://doi.org/10.1002/2015GC005732

Qi, B., Hu, D., Yang, X., Zhang, Y., Tan, C., Zhang, P., & Feng, C. (2016). Apatite fission track evidence for the Cretaceous–Cenozoic cooling history of the Qilian Shan (NW China) and for stepwise northeastward growth of the northeastern Tibetan Plateau since early Eocene. *Journal of Asian Earth Sciences*, *124*, 28–41. https://doi.org/10.1016/j.jseaes.2016.04.009

Ranalli, G. (1995). *Rheology of the Earth*. Springer Science and Business Media.

Royden, L. H., Burchfiel, B. C., & van der Hilst, R. D. (2008). The geological evolution of the Tibetan Plateau. *Science*, *321*(5892), 1054–1058. https://doi.org/10.1126/science.1155371

Schmeling, H., Babeyko, A. Y., Enns, A., Faccenna, C., Funiciello, F., Gerya, T., et al. (2008). A benchmark comparison of spontaneous subduction models—Towards a free surface. *Physics of the Earth and Planetary Interiors*, *171*(1–4), 198–223. https://doi.org/10.1016/j.pepi.2008.06.028

Schmidt, M. W., & Poli, S. (1998). Experimentally based water budgets for dehydrating slabs and consequences for arc magma generation. *Earth and Planetary Science Letters*, *163*(1–4), 361–379. https://doi.org/10.1016/S0012-821X(98)00142-3

Song, S., Zhang, L., Niu, Y., Su, L., Jian, P., & Liu, D. (2005). Geochronology of diamond-bearing zircons from garnet peridotite in the North Qaidam UHPM belt, northern Tibetan Plateau: A record of complex histories from oceanic lithosphere subduction to continental collision. *Earth and Planetary Science Letters*, *234*(1–2), 99–118. https://doi.org/10.1016/j.epsl.2005.02.036

Sun, L., Ji, J., Li, B., Li, X., Wu, W., & Zhang, K. (2022). Paleomagnetic constraints on Paleogene-Neogene rotation and paleo-stress in the northern Qaidam Basin. *Science China Earth Sciences*, 1–20. https://doi.org/10.1007/s11430-021-9949-1

Sun, Y., & Liu, M. (2018). Rheological control of lateral growth of the Tibetan Plateau: Numerical results. *Journal of Geophysical Research: Solid Earth*, *123*(11), 10–124. https://doi.org/10.1029/2018JB016601

Tapponnier, P., Zhiqin, X., Roger, F., Meyer, B., Arnaud, N., Wittlinger, G., & Jingsui, Y. (2001). Oblique stepwise rise and growth of the Tibet Plateau. *Science*, *294*(5547), 1671–1677. https://doi.org/10.1126/science.105978

Tunini, L., Jiménez-Munt, I., Fernandez, M., Vergés, J., Villaseñor, A., Melchiorre, M., & Afonso, J. C. (2016). Geophysical-petrological model of the crust and upper mantle in the India-Eurasia collision zone. *Tectonics*, *35*(7), 1642–1669. https://doi.org/10.1002/2016TC004161

Turcotte, D., & Schubert, G. (2014). *Geodynamics* (p. 456). Cambridge University Press.

Van Hinsbergen, D. J., Lippert, P. C., Dupont-Nivet, G., McQuarrie, N., Doubrovine, P. V., Spakman, W., & Torsvik, T. H. (2012). Greater India Basin hypothesis and a two-stage Cenozoic collision between India and Asia. *Proceedings of the National Academy of Sciences*, *109*(20), 7659–7664. https://doi.org/10.1073/pnas.1117262109

Vogt, K., Matenco, L., & Cloetingh, S. (2017). Crustal mechanics control the geometry of mountain belts. Insights from numerical modelling. *Earth and Planetary Science Letters*, *460*, 12–21. https://doi.org/10.1016/j.epsl.2016.11.016

Wang, W., Zhang, P., Garzione, C. N., Liu, C., Zhang, Z., Pang, J., et al. (2022). Pulsed rise and growth of the Tibetan Plateau to its northern margin since ca. 30 Ma. *Proceedings of the National Academy of Sciences*, *119*(8), e2120364119. https://doi.org/10.1073/pnas.2120364119

Wang, W., Zhang, P., Pang, J., Garzione, C., Zhang, H., Liu, C., et al. (2016). The Cenozoic growth of the Qilian Shan in the northeastern Tibetan Plateau: A sedimentary archive from the Jiuxi Basin. *Journal of Geophysical Research: Solid Earth*, *121*(4), 2235–2257. https://doi.org/10.1002/2015JB012689

Wilks, K. R., & Carter, N. L. (1990). Rheology of some continental lower crustal rocks. *Tectonophysics*, *182*(1–2), 57–77. https://doi.org/10.1016/0040-1951(90)90342-6

Xiao, Q., Shao, G., Yu, G., Cai, J., & Wang, J. (2016). Electrical resistivity structures of the Kunlun–Qaidam–Qilian system at the northern Tibet and their tectonic implications. *Physics of the Earth and Planetary Interiors*, *255*, 1–17. https://doi.org/10.1016/j.pepi.2016.03.011

Xie, R., Chen, L., Xiong, X., Wang, K., & Yan, Z. (2021). The role of Pre-existing crustal weaknesses in the uplift of the eastern Tibetan Plateau: 2D thermo-mechanical modeling. *Tectonics*, *40*(4), e2020TC006444. https://doi.org/10.1029/2020TC006444

Xu, Q., Zhao, J., Pei, S., & Liu, H. (2013). Distinct lateral contrast of the crustal and upper mantle structure beneath northeast Tibetan plateau from receiver function analysis. *Physics of the Earth and Planetary Interiors*, *217*, 1–9. https://doi.org/10.1016/j.pepi.2013.01.005

Yang, J. S., Xu, Z. Q., Zhang, J. X., Chu, C. Y., Zhang, R., Liou, J. G., et al. (2001). Tectonic significance of early Paleozoic high-pressure rocks in Altun-Qaidam-Qilian Mountains, northwest China. *Paleozoic and Mesozoic Tectonic Evolution of Central and Eastern Asia*, *194*, 141.

Yang, Y., Ritzwoller, M. H., Zheng, Y., Shen, W., Levshin, A. L., & Xie, Z. (2012). A synoptic view of the distribution and connectivity of the mid-crustal low velocity zone beneath Tibet. *Journal of Geophysical Research*, *117*(B4). https://doi.org/10.1029/2011JB008810

Ye, Z., Gao, R., Li, Q., Zhang, H., Shen, X., Liu, X., & Gong, C. (2015). Seismic evidence for the North China plate underthrusting beneath northeastern Tibet and its implications for plateau growth. *Earth and Planetary Science Letters*, *426*, 109–117. https://doi.org/10.1016/j.epsl.2015.06.024

Yin, A. (2010). Cenozoic tectonic evolution of Asia: A preliminary synthesis. *Tectonophysics*, *488*(1–4), 293–325. https://doi.org/10.1016/j.tecto.2009.06.002

Yin, A., Dang, Y. Q., Zhang, M., Chen, X. H., & McRivette, M. W. (2008). Cenozoic tectonic evolution of the Qaidam basin and its surrounding regions (Part 3): Structural geology, sedimentation, and regional tectonic reconstruction. *The Geological Society of America Bulletin*, *120*(7–8), 847–876. https://doi.org/10.1130/B26232.1

Yin, A., & Harrison, T. M. (2000). Geologic evolution of the Himalayan-Tibetan orogen. *Annual Review of Earth and Planetary Sciences*, *28*(1), 211–280. https://doi.org/10.1146/annurev.earth.28.1.211

Yin, A., Rumelhart, P. E., Butler, R., Cowgill, E., Harrison, T. M., Foster, D. A., et al. (2002). Tectonic history of the Altyn Tagh fault system in northern Tibet inferred from Cenozoic sedimentation. *The Geological Society of America Bulletin*, *114*(10), 1257–1295. https://doi.org/10.1130/0016-7606(2002)114<1257:THOTAT>2.0.CO;2

Yuan, D. Y., Ge, W. P., Chen, Z. W., Li, C. Y., Wang, Z. C., Zhang, H. P., et al. (2013). The growth of northeastern Tibet and its relevance to large-scale continental geodynamics: A review of recent studies. *Tectonics*, *32*(5), 1358–1370. https://doi.org/10.1002/tect.20081

Yue, H., Chen, Y. J., Sandvol, E., Ni, J., Hearn, T., Zhou, S., et al. (2012). Lithospheric and upper mantle structure of the northeastern Tibetan Plateau. *Journal of Geophysical Research*, *117*(B5). https://doi.org/10.1029/2011JB008545

Zhang, C., Guo, Z., & Chen, Y. J. (2020). Lithospheric thickening controls the ongoing growth of northeastern Tibetan Plateau: Evidence from P and S receiver functions. *Geophysical Research Letters*, *47*(15), e2020GL088972. https://doi.org/10.1029/2020GL088972

Zhang, P., Chen, L., Xiao, W., & Zhang, J. (2022). Topographic response of Hinterland Basins in Tibet to the India–Asia convergence: 3D thermo-mechanical modeling. *Front. Subduction and Collision Dynamics of Tectonic Plates*, *10*, 122. https://doi.org/10.3389/feart.2022.845126

Zhang, P. Z., Shen, Z., Wang, M., Gan, W., Burgmann, R., Molnar, P., et al. (2004). Continuous deformation of the Tibetan Plateau from global positioning system data. *Geology*, *32*(9), 809–812. https://doi.org/10.1130/G20554.1

Zhang, Z., Teng, J., Romanelli, F., Braitenberg, C., Ding, Z., Zhang, X., et al. (2014). Geophysical constraints on the link between cratonization and orogeny: Evidence from the Tibetan Plateau and the North China Craton. *Earth-Science Reviews*, *130*, 1–48. https://doi.org/10.1016/j.earscirev.2013.12.005

Zhao, J., Jin, Z., Mooney, W. D., Okaya, N., Wang, S., Gao, X., et al. (2013). Crustal structure of the central Qaidam basin imaged by seismic wide-angle reflection/refraction profiling. *Tectonophysics*, *584*, 174–190. https://doi.org/10.1016/j.tecto.2012.09.005

Zhao, W., Kumar, P., Mechie, J., Kind, R., Meissner, R., Wu, Z., et al. (2011). Tibetan plate overriding the Asian plate in central and northern Tibet. *Nature Geoscience*, *4*(12), 870–873. https://doi.org/10.1038/ngeo1309

Zheng, D., Zhang, P. Z., Wan, J., Yuan, D., Li, C., Yin, G., et al. (2006). Rapid exhumation at~ 8 Ma on the Liupan Shan thrust fault from apatite fission-track thermochronology: Implications for growth of the northeastern Tibetan Plateau margin. *Earth and Planetary Science Letters*, *248*(1–2), 198–208. https://doi.org/10.1016/j.epsl.2006.05.023

Zuza, A. V., Cheng, X., & Yin, A. (2016). Testing models of Tibetan Plateau formation with Cenozoic shortening estimates across the Qilian Shan–Nan Shan thrust belt. *Geosphere*, *12*(2), 501–532. https://doi.org/10.1130/GES01254.1

Zuza, A. V., Wu, C., Reith, R. C., Yin, A., Li, J., Zhang, J., et al. (2018). Tectonic evolution of the Qilian Shan: An early Paleozoic orogen reactivated in the Cenozoic. *Bulletin*, *130*(5–6), 881–925. https://doi.org/10.1130/B31721.1

Zuza, A. V., Wu, C., Wang, Z., Levy, D. A., Li, B., Xiong, X., & Chen, X. (2019). Underthrusting and duplexing beneath the northern Tibetan Plateau and the evolution of the Himalayan-Tibetan orogen. *Lithosphere*, *11*(2), 209–231. https://doi.org/10.1130/L1042.1

References From the Supporting Information

Burg, J. P., & Gerya, T. V. (2005). The role of viscous heating in Barrovian metamorphism of collisional orogens: Thermo-mechanical models and application to the Lepontine Dome in the central Alps. *Journal of Metamorphic Geology*, *23*(2), 75–95. https://doi.org/10.1111/j.1525-1314.2005.00563.x

Gehrels, G. E., Yin, A., & Wang, X. F. (2003). Detrital-zircon geochronology of the northeastern Tibetan plateau. *The Geological Society of America Bulletin*, *115*(7), 881–896. https://doi.org/10.1130/0016-7606(2003)115<0881:DGOTNT>2.0.CO;2

Gerya, T. V., & Yuen, D. A. (2003b). Rayleigh–Taylor instabilities from hydration and melting propel 'cold plumes' at subduction zones. *Earth and Planetary Science Letters*, *212*(1–2), 47–62. https://doi.org/10.1016/S0012-821X(03)00265-6

Hsü, K. J., Guitang, P., & Sengör, A. M. C. (1995). Tectonic evolution of the Tibetan Plateau: A working hypothesis based on the archipelago model of orogenesis. *International Geology Review*, *37*(6), 473–508. https://doi.org/10.1080/00206819509465414

Jackson, J. A., Austrheim, H., McKenzie, D., & Priestley, K. (2004). Metastability, mechanical strength, and the support of mountain belts. *Geology*, *32*(7), 625–628. https://doi.org/10.1130/g20397.1

Katz, R. F., Spiegelman, M., & Holtzman, B. (2006). The dynamics of melt and shear localization in partially molten aggregates. *Nature*, *442*(7103), 676–679. https://doi.org/10.1130/G20397.1

Pan, G. T., Mo, X. X., Hou, Z. Q., Zhu, D. C., Wang, L. Q., Li, G. M., et al. (2006). Spatial-temporal framework of the gangdese orogenic belt and its evolution. *Acta Petrologica Sinica*, *22*, 521–533. (in Chinese with English abstract).

Roger, F., Jolivet, M., & Malavieille, J. (2010). The tectonic evolution of the Songpan-Garzê (north Tibet) and adjacent areas from proterozoic to present: A synthesis. *Journal of Asian Earth Sciences*, *39*(4), 254–269. https://doi.org/10.1016/j.jseaes.2010.03.008

Rosenberg, C. L., & Handy, M. R. (2005). Experimental deformation of partially melted granite revisited: Implications for the continental crust. Journal of metamorphic. *Geology*, *23*(1), 19–28. https://doi.org/10.1111/j.1525-1314.2005.00555.x

Wang, Y., & Cheng, S. H. (2012). Lithospheric thermal structure and rheology of the eastern China. *Journal of Asian Earth Sciences*, *47*, 51–63. https://doi.org/10.1016/j.jseaes.2011.11.022

Wu, C., Yin, A., Zuza, A. V., Zhang, J., Liu, W., & Ding, L. (2016). Pre-Cenozoic geologic history of the central and northern Tibetan Plateau and the role of Wilson cycles in constructing the Tethyan orogenic system. *Lithosphere*, *8*(3), 254–292. https://doi.org/10.1130/L494.1

Zhu, D. C., Zhao, Z. D., Niu, Y., Mo, X. X., Chung, S. L., Hou, Z. Q., et al. (2011). The Lhasa terrane: Record of a microcontinent and its histories of drift and growth. *Earth and Planetary Science Letters*, *301*(1–2), 241–255. https://doi.org/10.1016/j.epsl.2010.11.005